Title
ELECTRICAL BREAKDOWN OF HYDROGEN ACROSS A STRONG MAGNETIC FIELD IN COAXIAL GEOMETRY

Author
Sherwood, Arthur Robert.

Publication Date
1967-03-28

UCRL-17178

University of California

Ernest O. Lawrence Radiation Laboratory

ELECTRICAL BREAKDOWN OF HYDROGEN
ACROSS A STRONG MAGNETIC FIELD IN COAXIAL GEOMETRY

Berkeley, California

DISCLAIMER

UCRL-17178

UNIVERSITY OF CALIFORNIA
Lawrence Radiation Laboratory
Berkeley, California

AEC Contract No. W-7405-eng-48

ELECTRICAL BREAKDOWN OF HYDROGEN ACROSS A STRONG MAGNETIC FIELD IN COAXIAL GEOMETRY

Arthur Robert Sherwood

(Ph. D. Thesis)

March 28, 1967

ELECTRICAL BREAKDOWN OF HYDROGEN
ACROSS A STRONG MAGNETIC FIELD IN COAXIAL GEOMETRY

Contents

ELECTRICAL BREAKDOWN OF HYDROGEN ACROSS A STRONG MAGNETIC FIELD IN COAXIAL GEOMETRY

Arthur Robert Sherwood

Lawrence Radiation Laboratory
University of California
Berkeley, California

March 28, 1967

ABSTRACT

The formative time of electric breakdown in low-pressure (0.2 to 2.0 torr) hydrogen across a strong magnetic field ($10 < \omega_b \tau < 350$; maximum B of 18 kG) has been measured in a coaxial cylindrical geometry. Attention was centered on that region of breakdown that occurs with a formative time less than the time required for an electron to drift across the electrode gap in the applied fields. This crossing time was inferred by extrapolations of previous measurements by Bernstein.

These formative time measurements are compared with a simplified theory which assumes a constant number of e-folding times until breakdown and neglects electron losses as well as secondary production at the cathode. This model predicts that the formative time is inversely proportional to the gas pressure and otherwise a function of only the ratio E/B and not of either field separately. The predicted pressure dependence is confirmed, but deviations from the predicted functional dependence on E/B are found. These deviations are attributed to electron losses along the magnetic field. Reasonable agreement with the predicted magnitude of the formative time is obtained.

I. INTRODUCTION

Under ordinary conditions a gas is a good, but not perfect, insulator. Very little current density will flow between cold electrodes placed in the gas when a potential difference is established between them as long as the potential difference is below a critical value, depending on the particular conditions, called the breakdown potential. If, however, the potential difference exceeds the breakdown potential, the gas rather abruptly ceases to be a good insulator and becomes instead a good conductor. This transitional process is called the electrical breakdown of the gas. It is accompanied by a large increase in the current flowing through the gas and by a collapse of the potential difference across the electrodes because of the impedance of the external circuit.

In general, if the potential difference exceeding the breakdown potential is suddenly established, there is a delay before the voltage collapses and the gas becomes a good conductor. This is shown schematically in Fig. 1. During this delay the voltage across the electrodes remains essentially constant at the applied value while the gas ionization and the current flowing through the gas build up. Here, the delay between the application of the potential and its collapse will be called the "formative time." The ionization buildup together with the rapid transition to some type of gas discharge (in other words, everything that happens from the establishment of the voltage until a gas discharge is obtained) will be called the "breakdown process" or simply the "breakdown."

Electrical breakdown occurs over a wide range of conditions, but here only direct current breakdown in uniform applied fields in a low pressure gas will be considered. For this case (and without a magnetic field) the following general description of the mechanism has emerged by which for moderate overvoltages the electrical current increases in the gas until the actual breakdown occurs. The picture has resulted from considerable theoretical and experimental attention that the subject has received over the years.[1-3]

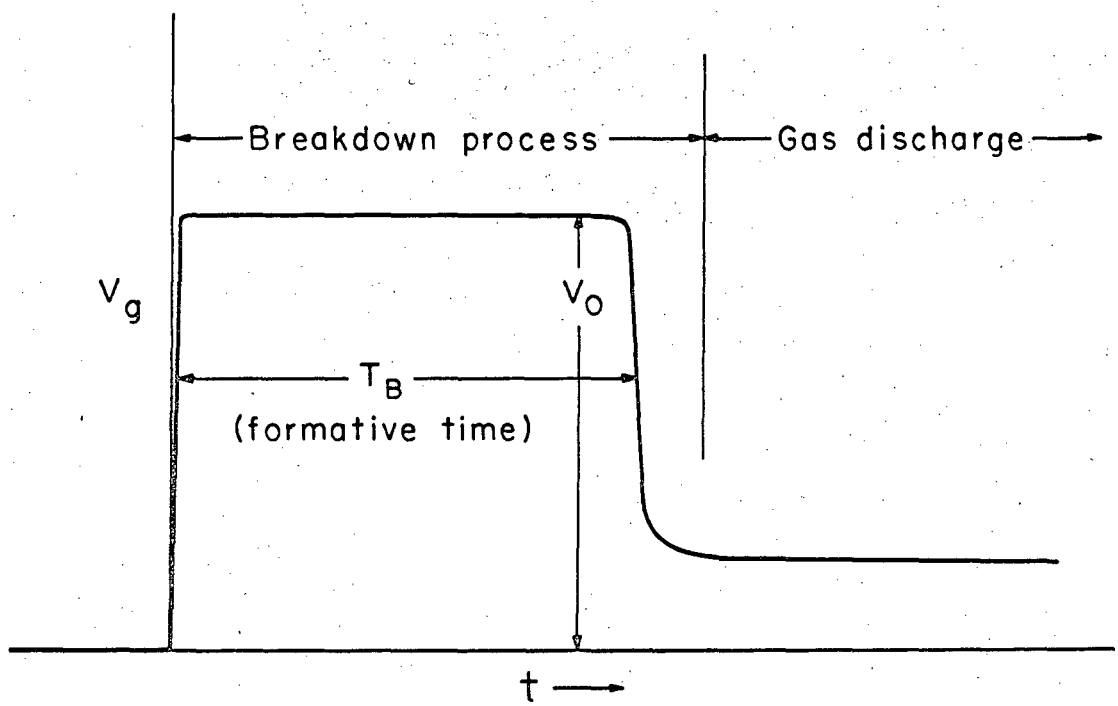

XBL673-2455

Fig. 1. Schematic diagram of the electrode voltage vs. time for an electrical breakdown process.

In addition to a sufficiently large electric field, for the breakdown process to occur it is also necessary that there be a few free electrons in the gas. When the potential difference is established across the electrodes these initial electrons produce primary (or first generation) electron avalanches by means of ionizing collisions with the gas. These primary avalanches are quenched at the anode, however, and the further growth of the ionization and of the current flowing in the gas depends entirely on the regenerative production of secondary electrons. Usually the secondary electron production at the cathode is the most important source. These secondary electrons, of course, produce second generation avalanches which are responsible for the eventual production of yet another generation of avalanches. The process continues until either the charged particle density becomes high enough that space charge effects become important and lead to a much more rapid rate of increase of the current, or else the current becomes so high that the potential between the electrodes falls because of the impedance of the external circuit. Whether or not space charge effects become important before voltage collapse begins depends on the impedance of the external circuit; but they must eventually occur in the final transition to a gas discharge. In general, the details of the processes by which the space charge affects the changing current are not known. Thus in the usual case of gas breakdown at low pressures the process is initiated by a few stray electrons which produce primary avalanches, then it is kept alive and growing by regenerative secondary electron production and is completed by means of space charge effects. This type of breakdown process is here called "multiple avalanche breakdown."

A deviation from the sequence of events just described can occur if the ionization rate is so high that a primary avalanche itself produces the voltage collapse. In this case the formative time is less than the time required for the primary avalanche to cross the electrode gap. Furthermore, the breakdown is controlled by the primary ionization processes and perhaps by the space charge induced processes, so that the secondary electron production processes play a lesser role.

Such a breakdown is here called the "primary avalanche breakdown." It is a particularly interesting case for study because it is essentially a volume process, being only weakly dependent on the surface effects which tend to dominate the secondary electron production. Primary avalanche breakdown in a uniform applied electric field and without an applied magnetic field has been obtained at high gas pressure (i.e. around one atmosphere) and with high overvoltages.[4]

In the present experiment the breakdown of hydrogen gas at low pressure (i.e. around one torr) across a strong magnetic field has been investigated by observing the formative time. The magnetic field was perpendicular to the applied electric field. The experiment was limited to the "strong magnetic field" (SMF), which is here defined as the case where the electron cyclotron frequency $\omega_b = eB/mc$ is much greater than the electron-neutral collision frequency for momentum transfer ν_c (including inelastic collisions). The ratio of these frequencies is denoted by $\omega_b\tau$. The strong magnetic field limit requires $\omega_b^2\tau^2 \gg 1$. In this investigation the range of the magnetic field was $6\ \text{kG} \leq B \leq 18\ \text{kG}$ and the pressure range was $0.2\ \text{torr} \leq p \leq 2.0\ \text{torr}$, so that the range of $\omega_b\tau$ was about $10 < \omega_b\tau < 350$.

Although breakdown across a strong magnetic field exhibits the same general characteristics as those described above for the case without magnetic field, the physical processes occurring during the breakdown process are considerably affected by the presence of the magnetic field. For example, the main drift motion of the electrons is in the $\vec{E} \times \vec{B}$ direction. Furthermore, the primary ionization process, the secondary electron production at the cathode, and any space charge effects are all strongly influenced by the effect of the magnetic field on the electron dynamics. In fact, the presence of the magnetic field made it possible to obtain primary avalanche breakdown at the low pressures of this experiment. Because this type of breakdown is especially interesting and is physically less complicated than the multiple avalanche type, the present investigation was essentially restricted to the primary avalanche breakdown case.

The electrode structure was of coaxial cylindrical geometry with the magnetic field in the axial direction and the electric field in the radial direction. The ratio of the radii of the electrodes was nearly unity; so to a good approximation the applied electric field was spatially constant.

Upon suddenly electrically connecting a charged capacitor across the electrodes, a measurement of the formative time for breakdown for a given set of the experimental parameters was obtained by observing the voltage across the electrode gap as a function of time. The measurements were compared with a simplified theory for proper functional dependence on the experimental parameters and also for the actual magnitude. In order to make the latter comparison it is necessary to use extrapolations from the experimental values of Bernstein for the electron drift velocity in the direction of the electric field[5] and for the first Townsend ionization coefficient.[6] Rough agreement between the measurements and the predictions of the simplified theory was obtained, although some deviation from a predicted functional dependence was found. The agreement is considered satisfactory, especially for an electrical breakdown experiment. The experiment thus provides a rough verification of Bernstein's measured value for the first Townsend ionization coefficient and reinforces his verification of the theoretical predictions of the behavior of electrons in a weakly ionized gas in a strong magnetic field.

The following mixed set of units is used unless otherwise stated whenever numerical relationships appear in the succeeding sections:

electric field	E	volts/cm
voltage	V	volts
magnetic field	B	kG
pressure	p	torr
length	x, r	cm
velocity	v	cm/sec
mass	m	g.

II. THEORY

A. The Model and Assumptions Employed

Due to the "primary avalanche" nature of the present investigation, the theory underlying the experiment is mainly that of the ionization buildup due to electrons moving under the influence of external fields through a cold neutral gas (hydrogen). The discussion presented here is for the model of a single avalanche leaving the cathode and growing by ionization as it moves across and around the gap. Electron attachment and recombination processes are negligible. Other electron losses from the growing avalanche are neglected for the nonce; they are discussed in Section V. The growth of the avalanche, then, is controlled by the ionization frequency β according to the relationship

$$N(t) = N_0 \exp\left[\int_0^t \beta(t')dt'\right], \qquad \text{(II-1)}$$

where $N(t)$ is the total number of electrons in the avalanche. β is an averaged quantity which accounts for all of the electrons.

The following restrictions are imposed upon this discussion:

(a) The distribution function for the gas molecules is constant in space and time.

(b) The applied electric and magnetic fields are perpendicular to each other, constant in time, and uniform in space.

(c) $\omega_b \tau \gg 1$.

(d) All speeds are nonrelativistic.

B. The Form of the Distribution Function

In order to determine β one needs to know the electron distribution function. For the densities involved during the formative time of the breakdown the electron-neutral collision frequency is much higher than the electron-electron collision frequency. Therefore the electron distribution function $f(\vec{r},\vec{v},t)$ is described by the Boltzmann equation

$$\frac{\partial f}{\partial t} + \nabla \cdot vf + \nabla_v \cdot \left[-\frac{e}{m}\left(\vec{E} + \frac{\vec{v}}{c} \times \vec{B}\right) f \right] = \left(\frac{\partial f}{\partial t}\right)_{coll} \qquad \text{(II-2)}$$

where $(\partial f/\partial t)_{coll}$ refers to collisions with molecules only and electron-electron collisions are neglected hereafter.

Since the gas molecules and the applied fields are uniform in space it is possible and desirable to eliminate the complication of the spatial dependence of the electron distribution function by integrating Eq. (II-2) over an appropriate volume, which is here the volume of the avalanche. Then the distribution function and quantities obtained from it are spatial averages.

In a "few" mean collision times after the initiation of an avalanche the electron distribution function reaches an "equilibrium" shape in velocity space where the energy gain due to elastic collisions in the crossed fields is balanced by the energy loss due to inelastic collisions. From then on the distribution function is of the form

$$f(\vec{v},t) = f(\vec{v}) \exp(\beta t). \qquad \text{(II-3)}$$

In the following discussion the distribution function will be assumed to be of this form. This amounts to the neglect of an initial transitory period. The time required for the distribution function to attain this form is of the order of the time required for an electron to gain sufficient energy to ionize a gas molecule. This time is now estimated for the most unfavorable combination of parameters in the present experiment. The average energy gain of an electron per elastic collision (neglecting molecular recoil) is about mv_d^2.[7] For $v_d = 3.3 \times 10^7$ cm/sec about 25 mean collision times are required for an electron to gain ionizing energy. Using a collision frequency of 4×10^9 p sec^{-1}, one finds that this takes about 3×10^{-8} sec at a gas pressure of 0.2 torr. Since the risetime of the gap voltage was 10^{-7} sec, using Eq. (II-3) is acceptable.

Notice that the use of Eq. (II-3) implies the following more simple form for Eq. (II-2):

$$N(t) = N_0 \exp(\beta t). \qquad \text{(II-4)}$$

Henceforth, the zero point in time is defined as the time when the potential across the electrode gap first reaches its full value. Thus the "initial" terms [such as N_0 in Eq. (II-4)] will contain the unknown "nonequilibrium" effects.

Having made the foregoing assumptions, the usual[8] method of solution of the Boltzmann equation is to expand the distribution function in spherical harmonics in velocity space

$$f(\vec{v}) = f^0(v) + \frac{\vec{v}}{v} \cdot \vec{f}^1(v) + \cdots \qquad \text{(II-5)}$$

and assume the convergence is sufficiently rapid that only the first two terms need be retained. Pearson and Kunkel[7] have shown that this method is applicable to the crossed field case as long as the mean electron kinetic energy is large compared to $1/2\ mv_d^2$, because then the electron distribution function is still sufficiently isotropic in the laboratory frame for the expansion to converge rapidly. In the present experiment the range of v_d was 3.3×10^7 cm/sec $\leq v_d \leq$ 6.6×10^7 cm/sec. Extrapolating the results of Bernstein[5] and/or using the results of the machine calculation of Pearson and Kunkel for hydrogen,[9] one obtains the following estimates for the mean electron energy $\bar{\epsilon}$:

v_d	$1/2\ mv_d^2$	$\bar{\epsilon}$
3.3×10^7 cm/sec	0.3 eV	$\approx$ 10 eV
6.6×10^7 cm/sec	1.2 eV	$\approx$ 20 eV

Therefore, it is concluded that the treatment of the Boltzmann equation as given by Allis[8] can be used here.

In general the function $f^0(v)$ cannot be determined exactly because of a lack of detailed knowledge of all the relevant cross sections. In addition to elastic collisions other contributing processes are molecular ionization, dissociation, electronic excitation, vibrational excitation, and rotational excitation. Qualitatively it seems reasonable that the elastic collisions tend to make the distribution function Maxwellian, whereas the inelastic collisions tend to increase the low

energy population at the expense of the "tail" of the distribution. Pearson and Kunkel[9] have performed a rough machine calculation for $f^0(v)$ in hydrogen using approximate cross sections, and they find this to be the case in their model.

C. Moments of the Distribution Function and Transport Coefficients

Despite the uncertainty in the distribution function it is useful to proceed. From the usual method, then, one obtains[8]

$$N(t) = 4\pi \exp(\beta t) \int_0^\infty v^2 f^0(v)\,dv \qquad \text{(II-6)}$$

$$v_E = \frac{\frac{1}{3}\frac{eE}{m}\int_0^\infty \frac{\nu_c}{(\nu_c^2 + \omega_b^2)} v^3 \frac{\partial f^0}{\partial v}\,dv}{\int_0^\infty v^2 f^0(v)\,dv} \qquad \text{(II-7)}$$

$$v_d = \frac{\frac{1}{3}\frac{eE}{m}\int_0^\infty \frac{\omega_b}{(\nu_c^2 + \omega_b^2)} v^3 \frac{\partial f^0}{\partial v}\,dv}{\int_0^\infty v^2 f^0(v)\,dv} \qquad \text{(II-8)}$$

where v_E is the drift velocity in the direction of the electric field and v_d is the drift velocity in the $\vec{E} \times \vec{B}$ direction. In the strong magnetic field (SMF) limit ($\omega_b \gg \nu_c$) the drift velocities can be written as

$$v_E = \frac{\frac{1}{\omega_b^2}\frac{eE}{m}\int_0^\infty \left[\nu_c + \frac{1}{3}v\frac{\partial}{\partial v}\nu_c\right]v^2 f^0(v)dv}{\int_0^\infty v^2 f^0(v)dv} \qquad \text{(II-9)}$$

and

$$v_d = \frac{eE}{m}\frac{1}{\omega_b} = 10^5\frac{E}{B} \text{ cm/sec}, \qquad \text{(II-10)}$$

and in this limit $v_d \gg v_E$.

Furthermore, consideration of the spatial term in the Boltzmann equation yields expressions for the diffusion coefficients which in the SMF limit become[8]

$$D_{\parallel} = \frac{1}{3}\left\langle\frac{v^2}{\nu_c}\right\rangle \qquad \text{(II-11)}$$

$$D_E = \frac{1}{3}\frac{1}{\omega_b^2}\langle v^2\nu_c\rangle \qquad \text{(II-12)}$$

$$D_\perp = \frac{1}{3}\frac{1}{\omega_b}\langle v^2\rangle \qquad \text{(II-13)}$$

where

$$\langle G(v)\rangle \equiv \frac{4\pi\int_0^\infty G(v)v^2 f^0(v)dv}{\int_0^\infty v^2 f^0(v)dv}.$$

Since the gas molecules are essentially at rest compared to the electrons, the ionization rate β is given by

$$\beta = 4\pi n_g\int_0^\infty \sigma_i(v)f^0(v)v^3dv \qquad \text{(II-14)}$$

where n_g is the number density of the gas molecules and $\sigma_i(v)$ is the

cross section for ionization by electron impact. Pearson and Kunkel have shown[7,9] that $f^0(v)$ and β/n_g both depend only on the drift velocity v_d in the SMF limit once the electron distribution function obtains the form of Eq. (II-3). Additional concepts necessary for the understanding of their argument are presented in Section II F; further discussion of this matter will be found there. Here, however, the following points are mentioned:

(1) By "depends only on v_d" or by "function only of v_d" it is meant that the parameters E and B only appear in the combination E/B and that there is no functional dependence on the gas pressure p (or equivalently n_g). There is no dependence on E/p or on $\omega_b\tau$ except in the combination $(E/p)/(\omega_b\tau)$.

(2) While the functional dependence

$$f^0(v) = G(v;v_d) \tag{II-15}$$

is only as accurate as the harmonic expansion for the distribution function, the relation

$$\frac{\beta}{n_g} = F_1(v_d) \tag{II-16}$$

is satisfied to much higher order. G and F_1 denote unspecified functions.

(3) The restrictions imposed in part A of this section are also imposed upon the cited work of Pearson and Kunkel. Their argument leading to Eqs. (II-15) and (II-16) depends on the additional assumptions: (a) The electron collisional scattering is independent of the azimuthal angle about the direction of the incident velocity, and (b) the electrons have random phases with respect to the azimuthal angle about the magnetic field. These assumptions are quite reasonable for the present discussion.

(4) It is evident physically that the electron distribution function must obtain the form of Eq. (II-3) before the functional dependence of Eq. (II-16) can hold, because before then the shape of the distribution function is time dependent.

D. Simplified Expressions for v_E and β

From Eqs. (II-9) and (II-10) it can be seen that if ν_c is independent of velocity

$$\frac{v_e}{v_d} = \frac{1}{\omega_b \tau} \qquad \text{(II-17)}$$

which yields

$$v_E = \frac{10^5}{\omega_b \tau} \frac{E}{B} \text{ cm/sec.} \qquad \text{(II-18)}$$

Bernstein has measured this ratio of drift speeds directly in the range 0.5×10^6 cm/sec $< v_d < 7.5 \times 10^6$ cm/sec and has found it to be constant when v_d is above about 5×10^6 cm/sec.[5] The result of the machine calculation of Pearson and Kunkel for $(v_E/v_d)\omega_b\tau$ (except for a numerical factor) is reproduced here as Fig. 2. It is seen that their results give a slight dropping off for the velocity ratio in the range of interest. (The cross-hatched area indicates the uncertainties present because of inexact knowledge of the collision frequencies for some of the inelastic processes.) From this calculation and from Bernstein's measurements it is concluded that Eq. (II-18) may be used as a reasonable approximation for the present experiment. Using Bernstein's constant experimental value for the drift velocity ratio one obtains the following approximate values:

$$v_E \approx 2.9 \times 10^4 \frac{p_0 E}{B^2} \text{ cm/sec} \qquad \text{(II-19)}$$

$$\omega_b \tau \approx 3.5 \frac{B}{p_0} \qquad \text{(II-20)}$$

where p_0 is the pressure at 20°C. The time required for an electron to cross the electrode gap will be denoted as T_c. An estimate for T_c obtained from Eq. (II-19) is

$$T_c \equiv \frac{d}{v_E} \approx 35 \frac{dB^2}{p_0 E} \text{ μsec} \qquad \text{(II-21)}$$

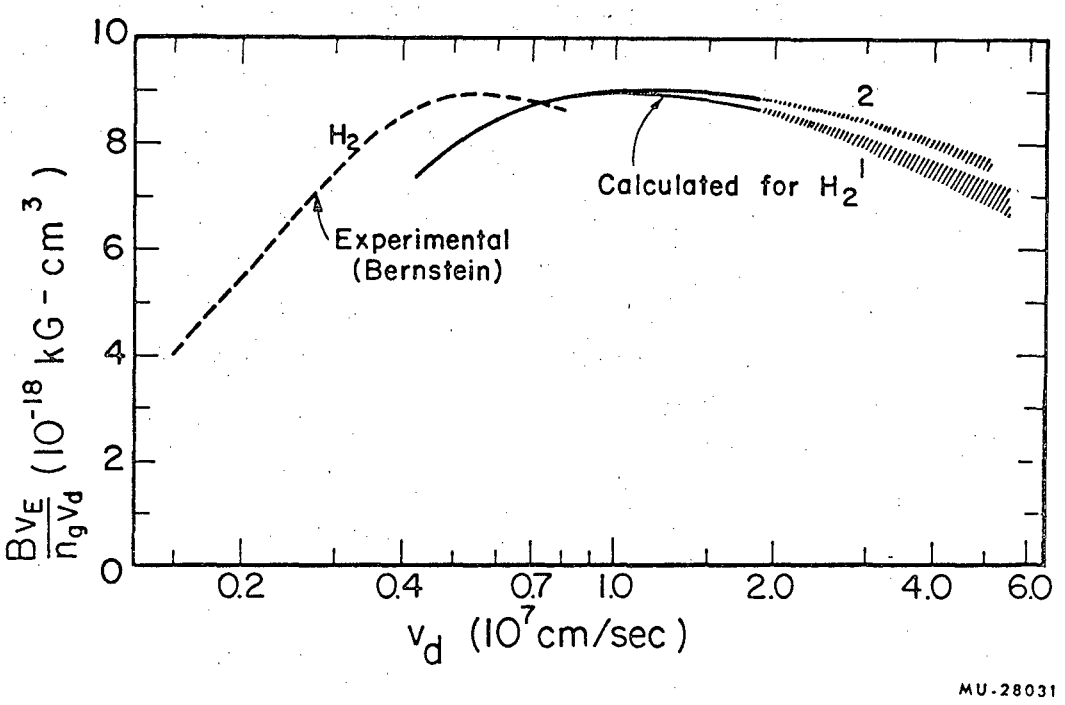

Fig. 2. The ratio of the drift velocities according to the calculation of Pearson and Kunkel.[9] Curves (1) and (2) are for different possible collision frequencies for electronic excitation.

where d is the gap length.

Applying these expressions rigorously to the present experiment, of course, involves a considerable extrapolation from Bernstein's measurements as can be seen by comparing the ranges of v_d given earlier for the two cases. Equation (II-17) can still be regarded as giving an "order of magnitude" relationship when one does not wish to assume that ν_c is independent of velocity.

It is seen from Eq. (II-14) that in order to obtain β it is necessary to know $\sigma_i(v)$ and also the electron distribution function. Unfortunately, in the present case where the inelastic processes are important the latter is unknown. There is available, however, in the unpublished work of Pearson and Kunkel[9] a calculation of β/n_g as a function of v_d. Their result for this function, which is reproduced here as Fig. 3, is somewhat uncertain because of incomplete knowledge of some of the cross sections. (The curves (1) and (2) in Fig. 3 result from different possible cross sections for the electronic excitation process.)

It is instructive to obtain an independent approximate expression for β by means of the first Townsend ionization coefficient α. In this way use can be made of the experimental values for α in the presence of an applied magnetic field and also of the wealth of experimental work for α in hydrogen with zero magnetic field.

The first Townsend ionization coefficient is defined to be the average number of new electrons created by a single electron as it traverses a unit length in the direction of the electric field.[10] From this definition it follows that α is related to β by the expression

$$\beta = \alpha v_E. \qquad \text{(II-22)}$$

An excellent discussion of the first Townsend ionization coefficient for the case of zero magnetic field is given by Loeb.[10] In this case α/p for a given gas is a function of E/p only. An empirical relation for this function,

$$\frac{\alpha}{p} = C_1' \exp\left(- C_2' \frac{p}{E}\right) \qquad \text{(II-23)}$$

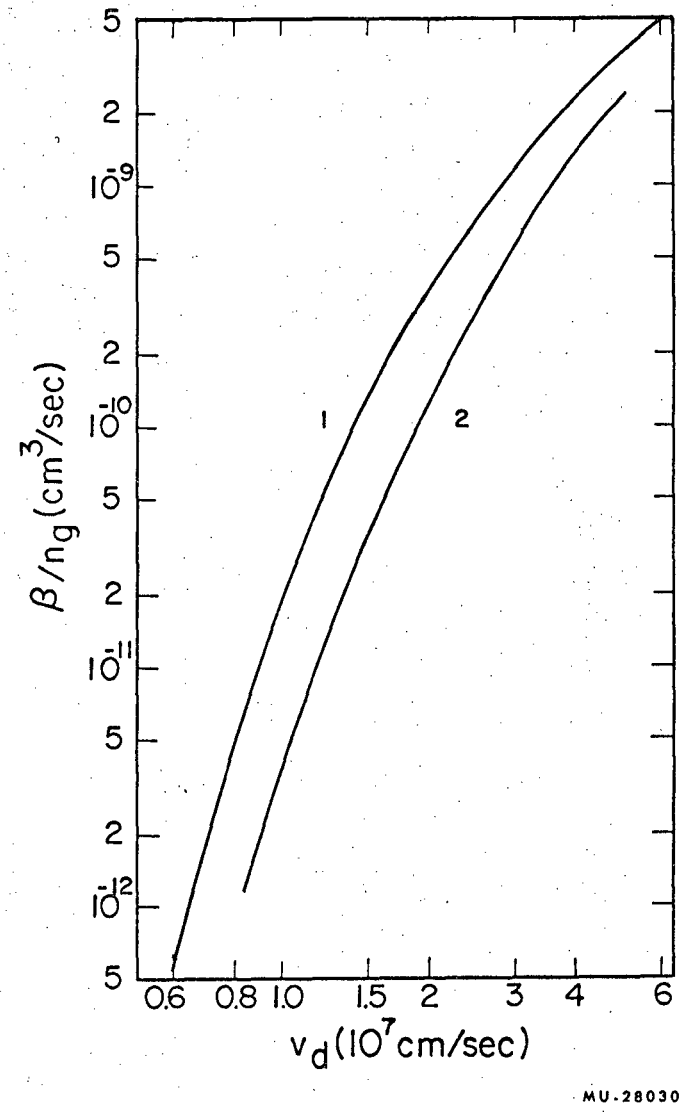

Fig. 3. β/n_g according to the calculation of Pearson and Kunkel.[9]

is well known. For hydrogen the constants C_1' and C_2' can be chosen so that Eq. (II-23) fits the experimental data well over a limited range of E/p. A more general expression for α/p can be obtained by combining Eq. (II-14) and Eq. (II-22). Doing so yields

$$\frac{\alpha}{p} = \frac{K}{v_E} \int_0^\infty \sigma_i(v) f^0(v) v^3 dv \qquad \text{(II-24)}$$

where K is a constant.

Blevin and Haydon[11] have obtained a theoretical form for α/p in the case of an applied magnetic field by considering the effect of the magnetic field on the quantities on the right hand side of Eq. (II-24). Their treatment employed two assumptions which are not really applicable in the present discussion, namely:

(1) The electron distribution function is Maxwellian.

(2) ν_c is independent of velocity.

Nevertheless, it is instructive to compare Eq. (II-16) with the generalization that they have obtained for Eq. (II-23). It is

$$\frac{\alpha}{p} = C_1'(1 + \omega_b^2\tau^2)^{1/2} \exp\left[- C_2' \frac{p}{E} (1 + \omega_b^2\tau^2)^{1/2}\right]. \qquad \text{(II-25)}$$

From Eq. (II-25) it is seen that with their assumptions Blevin and Haydon have found that formally the effect of the magnetic field is the same as if there were no magnetic field and the pressure were increased to $p(1 + \omega_b^2\tau^2)^{1/2}$. Obviously Eq. (II-25) reduces to Eq. (II-23) when the magnetic field vanishes.

In the SMF limit, on the other hand, Eq. (II-25) becomes

$$\frac{\alpha}{B} = C_1 \exp\left(- C_2 \frac{B}{E}\right). \qquad \text{(II-26)}$$

In the present discussion this equation is used in the same spirit as Eq. (II-23) is used in the zero magnetic field case. That is, Eq. (II-26) is regarded as an empirical relation in which the constants C_1 and C_2 can be chosen such that good agreement with experimental values over a limited range of v_d is obtained.

To the author's knowledge, however, there are no measurements for α/p in a magnetic field at high $\omega_b\tau$ in the range of v_d of interest here. This situation arises because α/p is usually measured in the steady state at prebreakdown conditions, and the present experiment is concerned with conditions so far beyond breakdown threshold that single avalanche breakdown occurs. It is thus necessary to employ the further approximation of using values of C_1 and C_2 measured for different conditions than those of this experiment. This can be done either by (1) combining the values of C_1' and C_2' for hydrogen obtained by Rose[12] and others[6,13] for B = 0 and E/p up to 1000 volts cm^{-1} $torr^{-1}$ with Eq. (II-20) from Bernstein's drift velocity measurements,[5] or by (2) using the values for C_1 and C_2 measured by Bernstein[6] using data mainly at low B, E/p, and $\omega_b\tau$ but extending up to $\omega_b\tau$ = 11 and $v_d = 2 \times 10^6$ cm/sec, or by (3) fitting Eq. (II-26) to the corresponding function calculated by Pearson and Kunkel.

The first method has the advantage of employing the "closest" available experimental data in that Eq. (II-20) uses measurements at $v_d = 7 \times 10^6$ cm/sec, but it has the disadvantage of using Eq. (II-25) and thus introducing the inappropriate assumptions of Blevin and Haydon. The second method suffers from the fact that most of Bernstein's data is for conditions far removed from those of this experiment (for half of his data the SMF limit cannot be applied); but it has the advantage of being a straightforward extrapolation from actual measurements of the ionization coefficient in a magnetic field. Finally, the third method is somewhat unsatisfactory because of the uncertainties in the calculation as mentioned before.

The three methods give, respectively:

(1) $C_1 = 19$ cm^{-1} kG^{-1}; $C_2 = 522$ volts cm^{-1} kG^{-1}

(2) $C_1 = 30$ cm^{-1} kG^{-1}; $C_2 = 778$ volts cm^{-1} kG^{-1}

(3) $C_1 = 27$ cm^{-1} kG^{-1}; $C_2 = 540$ volts cm^{-1} kG^{-1}.

The function α/B according to Eq. (II-26) with these three sets of constants is shown in Fig. 4. Also shown in Fig. 4 are (a) the results

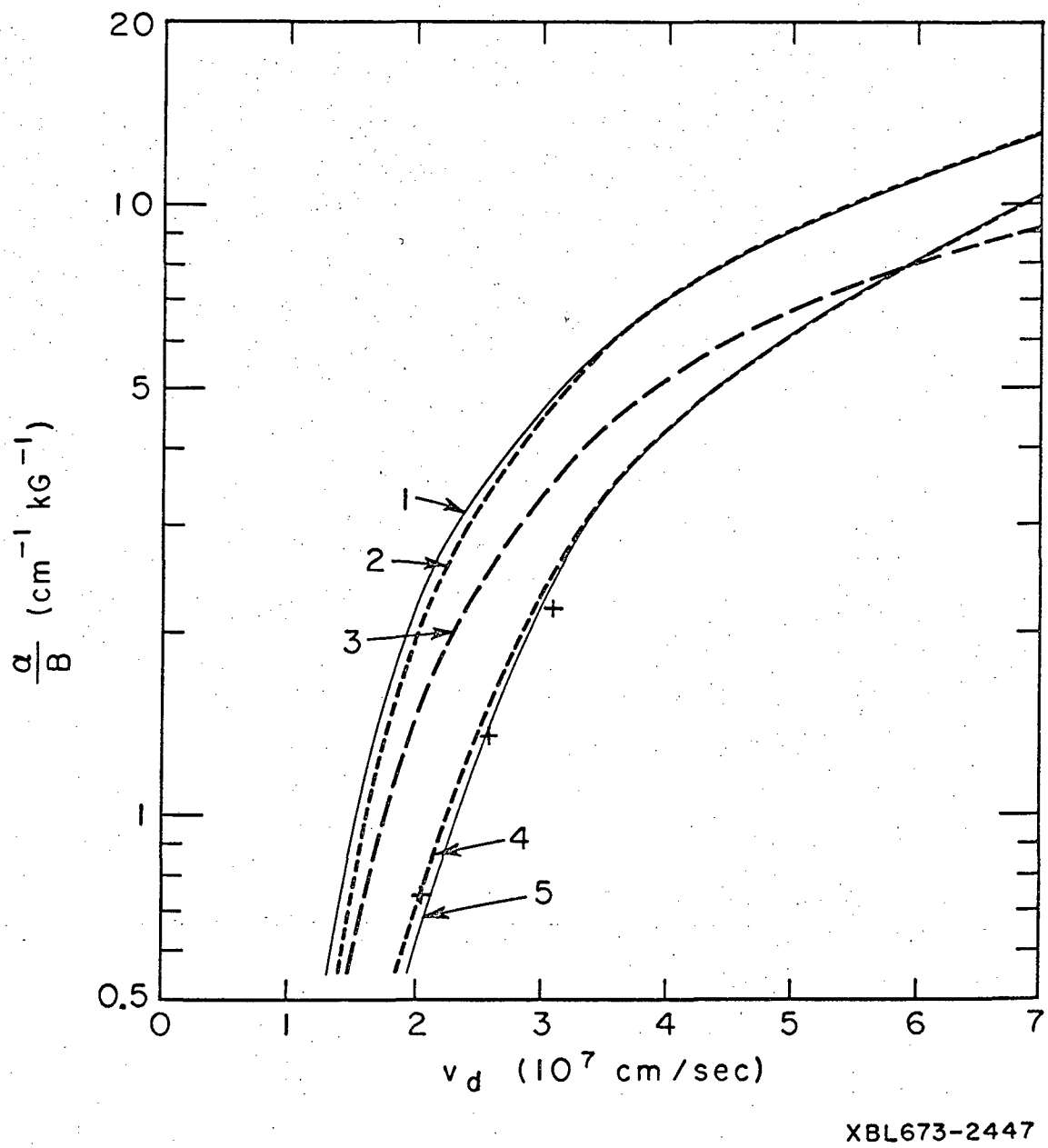

Fig. 4. Various estimates of the first Townsend ionization coefficient. (1) Pearson and Kunkel.[9] (2) 27 exp (-540 B/E). (3) 19 exp (-522 B/E). (4) Pearson and Kunkel with a cross section adjusted to fit curve 5. (5) 30 exp (-778 B/E). + The experimental values of Fletcher and Haydon[17] for $\omega_b\tau \approx 3.5$.

for this function obtained from the numerical calculation of Pearson and Kunkel (curve 1), (b) a second curve obtained by them to demonstrate that they could get agreement with the experimental values of Bernstein[6] by adjusting the magnitude of their adopted function for the cross section for electronic excitation (curve 4), and (c) some recent experimental values of Fletcher and Haydon[17] which are seen to agree fairly well with those of Bernstein.

Combining Eq. (II-26) with Eq. (II-22) and Eq. (II-19) one obtains finally the desired approximate expression for the ionization frequency:

$$\frac{\beta}{p_0} \approx 2.9 \times 10^4 \frac{E}{B} C_1 \exp\left(- C_2 \frac{B}{E}\right). \qquad \text{(II-27)}$$

Notice that this expression is of the expected form in that β/n_g is a function of v_d only.

Figure 5 shows curves of β/n_g obtained from Eq. (II-27) for the three sets of the constants C_1 and C_2. (The relation between p_0 and n_g is taken to be: $n_g = 3.30 \times 10^{16} p_0$ cm^{-3}.) Also shown for comparison in Fig. 5 are the two curves of Fig. 3. The labeling of the curves in Fig. 5 corresponds to that in Fig. 4; identically labeled curves are related by Eq. (II-22). In obtaining β from α Pearson and Kunkel have used their results for v_E shown in Fig. 2 and therefore did not assume that v_E/v_d is constant. Equation (II-19) is used in obtaining the other curves for β, and therefore for them the assumption of a constant drift velocity ratio is employed. This difference in procedure results in the separation in Fig. 5 of the curves that matched (over the experimental range of v_d) in Fig. 4. Specifically, the droop of the drift velocity ratio at higher v_d in Fig. 2 causes the β curves of Pearson and Kunkel in Fig. 5 to tend to drop off with respect to the others in the upper range of v_d.*

It is seen from Fig. 5 that the three approximations obtained

---

*The numerical calculation of Englehardt and Phelps[20] is for values of v_d too low to apply to this experiment. Where it does overlap, however, this calculation agrees well with curve (1) of Fig. 5.

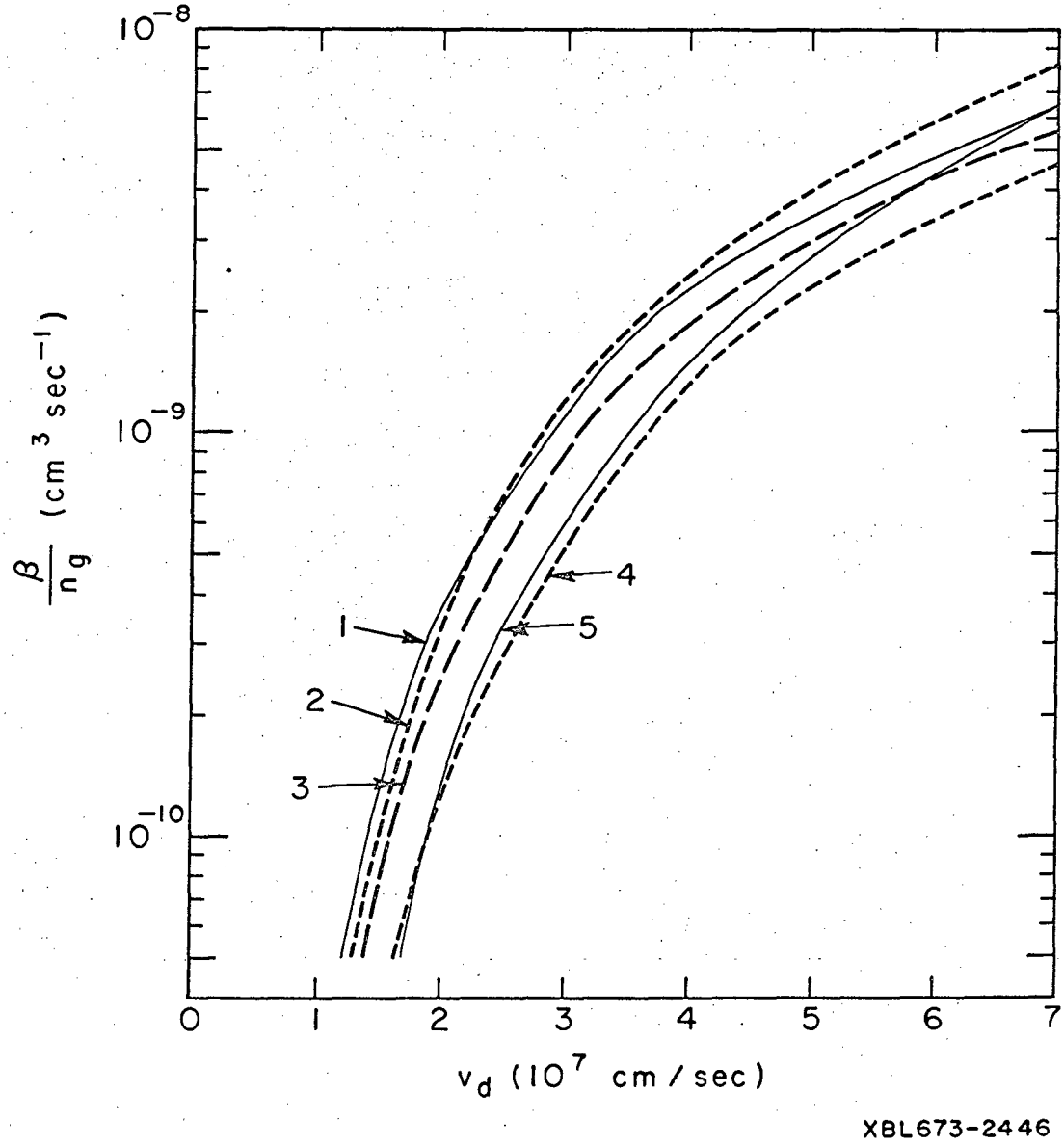

Fig. 5. The ionization frequency β for the five cases in Fig. 4. The curve labels here are the same as for that figure.

from Eq. (II-26) and the two curves of Pearson and Kunkel all form a "band" of values for β/n_g. For order-of-magnitude estimates in the range of the experiment any of the approximations will suffice. However, the question still remains as to which is the "best" approximation for β to be used to obtain predicted formative times for comparison with the experimental data. For the present curve 3 ot Fig. 5, which is given by the expression

$$\frac{\beta}{n_g} = 16.7 \times 10^{-12} \frac{E}{B} \exp\left(-522 \frac{B}{E}\right) \text{cm}^3 \text{ sec}^{-1}, \qquad \text{(II-28)}$$

is arbitrarily chosen. In Section IV the question is turned around and discussed from the viewpoint of using the experimental results to decide which is the best approximation for β.

E. The Formative Time

There still remains the problem of relating the formative time to the ionization rate. In the experiment the formative time was defined as the interval between the establishment of the potential across the electrodes and its sudden collapse. To discuss the significance of this voltage collapse requires consideration of the external discharge circuit. Figure 6 shows the essential elements of the discharge circuit. (The complete circuit diagram is shown in Fig. 12 and is discussed in Section III.) In Fig. 6 the electrode gap is represented by a capacitor in parallel with a variable impedance.

The capacity of the main (or driving) capacitor C_0 was large compared to all other capacities. In fact, it was large enough that the voltage across it remained essentially constant during the formative time, although it finally began to fall at the end of the voltage collapse. Therefore, the voltage collapse occurred when the current flowing through the gas became large enough to cause an observable voltage drop across the series resistor R. (The contribution to the current flowing through the gas from the discharge of the electrode capacity itself was negligible, so essentially all of the current that flowed through the gas also went through the series resistor.) Because of the exponential nature of the current rise, the formative time is rather insensitive to the value of R.

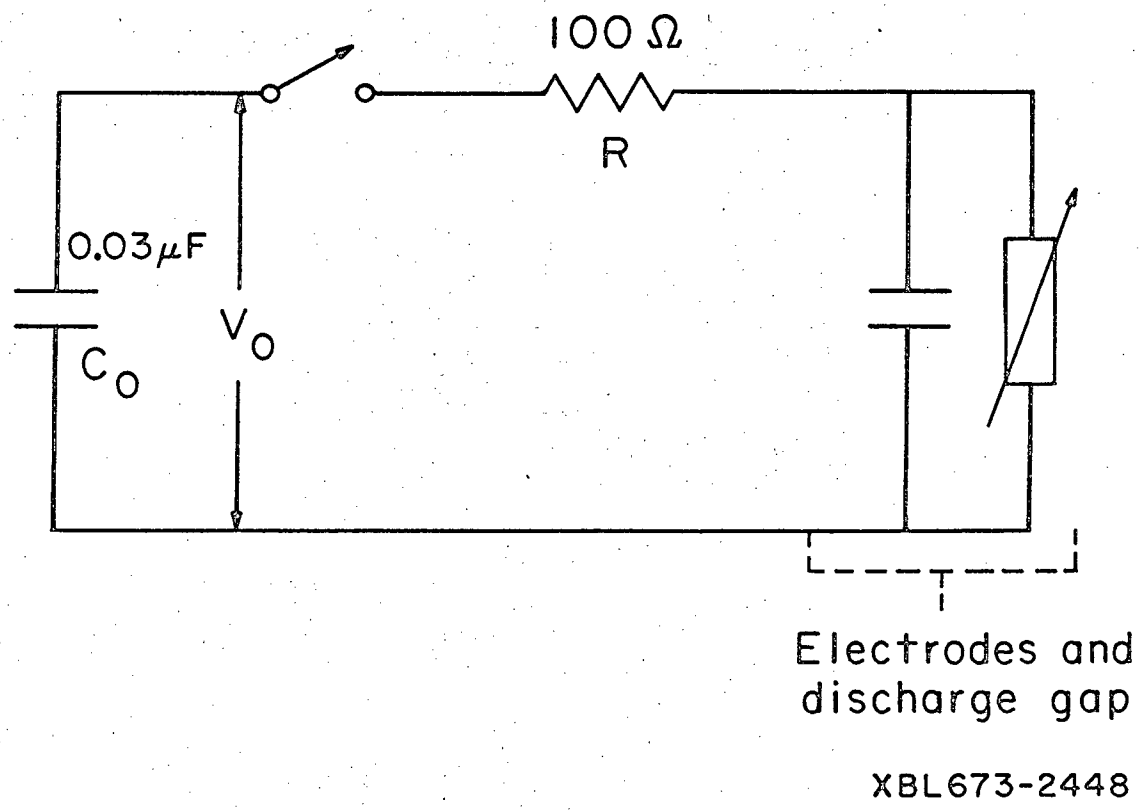

Fig. 6. The essential elements of the discharge circuit.

For a primary avalanche breakdown, after the voltage appears across the discharge gap the current flowing through the gas and also N(t) increase as exp (βt) while β remains constant at a value determined by the applied fields and the gas pressure. Eventually, however, the current becomes high enough that the voltage collapses, and other physical mechanisms such as space charge effects become imporant as the final transition to a steady state gas discharge occurs.

One can distinguish between two cases depending upon the nature of the current rise at the onset of the voltage collapse. In one case (which will be called the "Townsend" case) at the onset of voltage collapse the current is still rising as exp (βt) with β having the same value it had early in the breakdown process. New physical effects do not become important until after the onset of voltage collapse. In this case the formative time is inversely proportional to the ionization rate,

$$T_B \sim \frac{1}{\beta} , \tag{II-29}$$

and so by Eq. (II-16) can be expressed in the form

$$T_B \sim \frac{1}{p} F\left(\frac{E}{B}\right) \tag{II-30}$$

where T_B is the formative time and F is an unspecified function.

In the other case, at a time when the current is still too low to produce an observable voltage drop the charged particle density in the gap becomes high enough that a new physical mechanism (such as space charge effects or a plasma instability) becomes dominant and causes a much higher ionization rate than before. Then the voltage collapse occurs very quickly after the onset of the new process, and T_B becomes a measure of the time until this onset. In this case the expression for T_B corresponding to Eq. (II-30) is determined by the conditions for the onset of the new process and in general would be expected to exhibit a more complicated dependence on the applied fields and the pressure. However, if the new mechanism is due to space charge effects or otherwise depends primarily on the charged particle density, then

T_B would still be inversely proportional to β and therefore have the functional dependence of Eq. (II-30) except perhaps for corrections due to diffusion effects. (Diffusion affects the volume of the avalanche and therefore the charge density, but its effect on T_B is weak because of the exponential nature of the avalanche growth.)

For the purpose of obtaining an expression for comparison with the experiment, Eq. (II-29) and therefore Eq. (II-30) will be assumed to be valid regardless of the breakdown mechanism. (It is understood that in this paper the symbol β refers to the constant ionization rate, determined by the gas pressure and the applied fields according to Eq. (II-16), that applies early in the breakdown process. The symbol $\beta(t)$ is used for the general case.)

Figure 11 shows copies of typical oscilloscope traces of the gap voltage versus time. Two cases are shown, one for which the onset of the voltage collapse was very sudden and one for which it was more gradual.

The range of the applied voltages over which primary avalanche breakdown was observed was 2.4 kV to 12.0 kV. Taking 5% as an "observable" voltage drop on the oscilloscope traces, the current flowing at the onset of the voltage collapse ranged from 1.2 A to 6.0 A.

It is of interest to calculate the values of βT_B that correspond to these "observable" currents according to the relation

$$\beta T_B = \ln\left[\frac{I(T_B)}{I_0}\right]. \qquad \text{(II-31)}$$

The values of βT_B so obtained apply to the experiment directly for the "Townsend" type of voltage collapse and represent an upper limit for the more complicated case where a new mechanism was involved. Unfortunately, the value of I_0 was unknown. A small area of the cathode was illuminated with ultraviolet light, but for reasons made apparent in Section III it was not possible to measure the photoelectric current. Furthermore, I_0 in Eq. (II-31) refers to the current that was flowing at the time at which the gap voltage first reached

its full value, and this current was larger than the photoelectric current because of the high electric field and because of the ionization that occurred during the voltage risetime. Noting that βT_B only depends logarithmically on I_0 anyway, a guess of 10^{-11} A for I_0 will be used. This is a more or less typical value for a photoelectric current in the absence of a magnetic field, and it is hoped that the decrease in the actual photoelectric current from the value due to the strong magnetic field (which returned the photoelectrons to the cathode unless they made a collision with a gas molecule first) was about balanced by the increase in the value of I_0 over the actual photoelectric current. Using 10^{-11} A for I_0, then, one finds that for "observable" currents ranging from 1.2 A to 6.0 A the range of βT_B was about 25.5 to 27. Obviously, an error of an order of magnitude in I_0 would shift βT_B by about 2.5.

Next it is of interest to estimate the number of charged particles that were present in the gap when the current became "observable" to see if space charge effects were likely to be important yet. An exact treatment will not be attempted, for a rough argument will suffice. First, it is necessary to consider the behavior of the ions during the avalanche growth. This subject is treated in Appendix B, and the results are quoted here. The dominant ion species was H_2^+. Although $\omega_b \tau$ was large for the electrons it was less than unity for the ions, and the drift motion of the ions was nearly straight toward the cathode. Usually the ion mobility was large compared to the electron mobility; that is $V_E \gg v_E$, where V_E is the drift velocity of the ions in the direction of the electric field. (V_E assumes its minimum and v_E assumes its maximum at the lowest values of $\omega_b \tau$; in this case V_E and v_E were comparable.) As a result, the electrical current through the gas at the end of the formative time was carried mainly by the ions. (Early in the breakdown process when the avalanche head was still close to the cathode this was not true because of the rapid ion removal.)

Therefore, to a good approximation over most of the range of the experiment, at the onset of the voltage collapse

$$I \approx \frac{N^i}{d} eV_E \qquad \text{(II-32)}$$

where N^i is the total number of ions in the gap and d is the gap length. A rough calculation in Appendix B gives the following expression for the ion drift velocity:

$$V_E \approx 10^5 \sqrt{\frac{E}{p_0}} \quad \text{cm/sec.} \qquad \text{(II-33)}$$

A typical value for V_E, then, was about 10^7 cm/sec. Again taking a 5% voltage drop as the criterion for the onset of voltage collapse, the current at time T_B was given by

$$I(T_B) = 5 \times 10^{-2} \frac{V_g}{R} \text{ amperes.}$$

Combining this expression with Eqs. (II-32) and (II-33), one obtains

$$N^i(T_B) \approx 3 \times 10^{10} d^2 \sqrt{Ep_0} \qquad \text{(II-34)}$$

for R = 100 Ω. (The units employed are those set forth at the end of Section I.)

The experimental range of the quantity $d^2\sqrt{Ep_0}$ was $3 \leq d^2\sqrt{Ep_0} \leq 99$. From Eq. (II-34) one then obtains 9×10^{10} to 3×10^{12} as the range for $N^i(T_B)$.

Although ion removal at the cathode occurs during the avalanche buildup, the exponential nature of the buildup implies that $N(T_B) \approx N^i(T_B)$. Furthermore, because of the different directions of the electron and ion drift motions and because of the high value of V_E, the electrons and the ions become separated both in the direction of $\vec{E}$ and in the direction of $\vec{E} \times \vec{B}$. Therefore, the magnitude of the space charge field due to a quantity of electrons equal to $N^i(T_B)$ should give a reasonable estimate for the space charge fields that were actually present. To obtain a lower limit for these fields it will be assumed that these electrons were uniformly spread throughout the gap except in the direction of the electric field where they occupied

a band of some small thickness. With this assumption, the space charge fields to be expected were about

$$\Delta E \approx 3 \times 10^{-9} N^{i}(T_B) \quad \text{volts/cm},$$

or about 300 volts/cm to 10 000 volts/cm. The lower limit here is about an order of magnitude lower than the applied fields that led to this value. Nevertheless fields of such magnitude would be expected (at the least) to have a significant effect on the ionization rate because β is a rather strong function of E at constant p and B. (See Fig. 5.) The upper limit is quite comparable to the applied electric field that led to it (12 000 volts/cm) and so represents significant space charge distortion of the applied field.

It is to be emphasized that the point of the preceding paragraphs was to establish that over most of the range of the experimental parameters by the time the voltage drop was observable on the oscilloscope traces space charge effects must have been present. The possible exceptions were the cases of lowest gap voltages.

It was the lowest gap voltage, however, which led to the lowest value in the estimated range for βT_B. It is therefore concluded that a reasonable estimate for the value of βT_B is 25.5. Combining $\beta T_B = 25.5$ [which involves the assumption expressed by Eq. (II-29)] with Eq. (II-27), one obtains as a prediction for the formative time

(1) $$T_B \approx 46 \frac{1}{p_0} \frac{B}{E} \exp\left(522 \frac{B}{E}\right) \ \mu\text{sec} \qquad \text{(II-35)}$$

(2) $$T_B \approx 29 \frac{1}{p_0} \frac{B}{E} \exp\left(778 \frac{B}{E}\right) \ \mu\text{sec} \qquad \text{(II-36)}$$

(3) $$T_B \approx 33 \frac{1}{p_0} \frac{B}{E} \exp\left(540 \frac{B}{E}\right) \ \mu\text{sec} \qquad \text{(II-37)}$$

depending upon which set of constants C_1 and C_2 that one uses.

F. A Physical Picture

In this section a physical picture of the behavior of the electrons in the crossed fields is presented. Two particular frames of reference are especially convenient for the discussion. The electron motion in these two reference frames is illustrated in Fig. 7.

The Laboratory Frame

In the present discussion the neutral gas is at rest with respect to the electrode structure; therefore the laboratory frame and the reference frame in which the mean velocity of the gas molecules vanishes are identical.

It is well known that for $\omega_b \tau \gg 1$ the motion of an electron between collisions in uniform crossed electric and magnetic fields consists of a constant translation along B and a cycloidal motion in the plane normal to B, assuming $E < B$. The electron makes many cyclotron revolutions between each collision, so when it does collide with a gas molecule its phase in its orbit is random. In each collision the momentum transfer causes the electron's guiding center to jump discontinuously (in the sense that the collision is a discontinuous process). On the average the momentum transfer collisions cause the electron to have a net drift motion antiparallel to the electric field.

An electron born at rest acquires an energy of mv_d^2 from the electric field. Its kinetic energy is not constant, but rather it oscillates in value as the electron moves up and down the electric field in its orbit. However, since the electron's motion consists of the drift velocity v_d superimposed on the circular cyclotron motion of speed v_d, it is often convenient to consider the electron's energy gain as being $1/2\ mv_d^2$ of drift energy and $1/2\ mv_d^2$ of thermal energy.

Similarly, as an electron moves through the gas occasionally colliding with a molecule on the average it gains an energy of mv_d^2 from the electric field per momentum transfer collision, neglecting molecular recoil. As before, the electron's energy can be considered as being $1/2\ mv_d^2$ of drift energy and some thermal energy. The momentum transfer collisions randomize the drift energy, but following each collision the electron gains back its drift energy and also on the

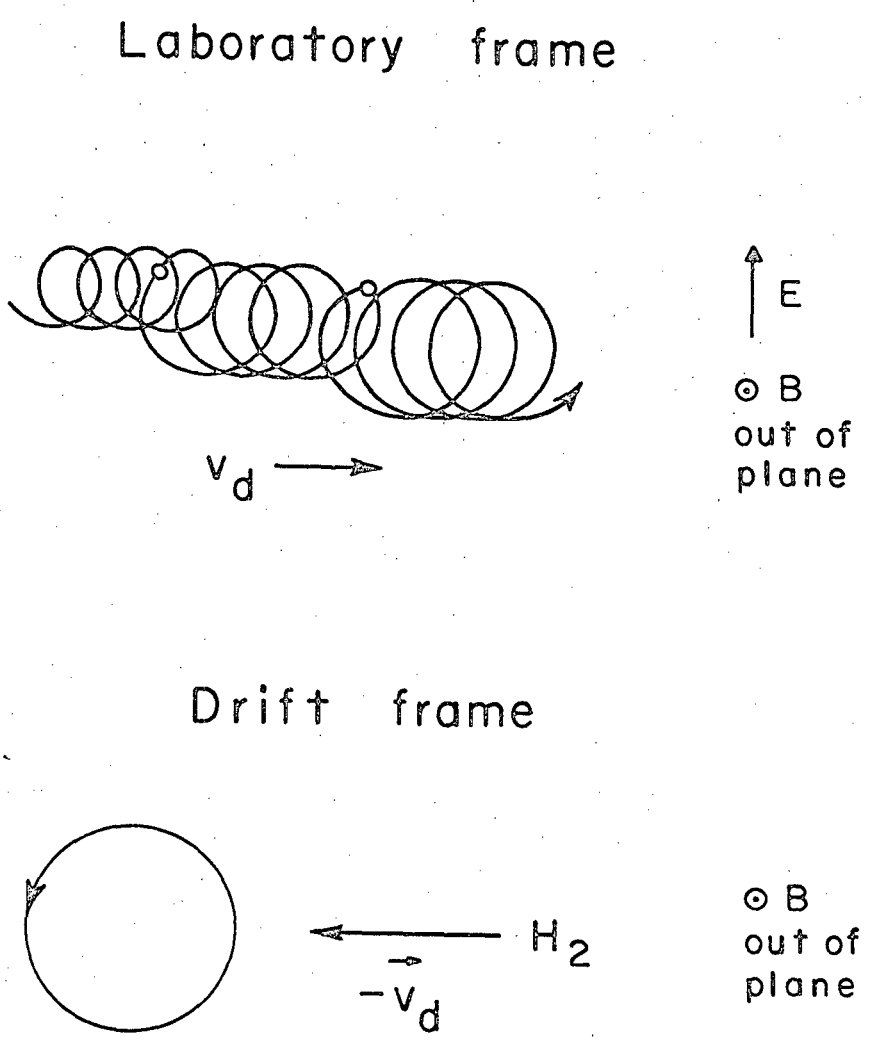

Fig. 7. The orbit of an electron in the laboratory frame of reference and in the drift frame of reference. In the laboratory frame the neutral gas is at rest; in the drift frame it flows with velocity $-v_d$.

average another 1/2 mv_d^2 of thermal energy. Of course if the collision is inelastic the electron will first lose some of its energy to the molecule, but then it still, on the average, gains back mv_d^2 from the electric field.

Obviously the electron's drift velocity antiparallel to the electric field and its energy gain from the electric field are very closely related to each other. This drift motion is responsible for the average energy gain.

The motion of a whole cloud of electrons follows from the above description of the behavior of a single electron. The cloud drifts in the $\vec{E} \times \vec{B}$ direction with velocity v_d. In addition it drifts antiparallel to the electric field with velocity v_E, which is of order $v_d(\omega_b\tau)^{-1}$. Actually, the drift velocity in the $\vec{E} \times \vec{B}$ direction is not quite v_d. There is a small correction of order $v_d(\omega_b\tau)^{-2}$ which can be ascribed to frictional drag by the gas on the moving cloud of electrons. The momentum transfer collisions cause the cloud to heat up, but it is also cooled by inelastic collisions with the gas molecules. The diffusion of the cloud is greatest along the magnetic field, for D_E is of order $D_{\|}(\omega_b\tau)^{-2}$. Thus the cloud has a different scale length along the magnetic field than it has in the other two directions.

The electron velocity distribution function is essentially spherical, but the center of the sphere is offset from the origin in velocity space by the two drift velocities v_d and v_E. The heating of the electrons can be described as an isotropic diffusion of the distribution function in velocity space.[7]

The Drift Frame

The drift frame is the frame of reference in which the electric field vanishes. It moves at a velocity of $\vec{v}_d$ with respect to the laboratory frame.

In the drift frame an electron's motion between collisions consists of a uniform translation along the magnetic field and a circular gyration in the plane normal to B. The cold gas flows with velocity

$-\vec{v}_d$ perpendicular to the magnetic field. In this frame the electron's drift velocity of magnitude v_E and its average energy gain are due to the gas wind rather than to an electric field. In addition there is a small drift velocity of order $v_E(\omega_b\tau)^{-1}$ in the direction of the wind of neutral gas. This latter drift can be considered to be due to frictional drag with the wind, and it corresponds to the small correction to the $\vec{E} \times \vec{B}$ drift in the laboratory frame.

The condition $\omega_b\tau \gg 1$ implies that the electron has random phase in its circular orbit when it collides with a gas molecule. On the average the light electron will experience a larger momentum transfer, and therefore a larger shift in the position of its guiding center, if it collides on that part of its circular orbit where it is moving against the heavy gas wind than if it collides where it is moving in the same direction as the wind. This effect causes the electron to have a net drift in the $\vec{B} \times (-\vec{v}_d)$ direction, which is the same as the drift against the electric field in the laboratory frame.

In the drift frame the kinetic energy of an electron is constant between collisions. (This is one of the most convenient features of this frame.) Elastic collisions with the gas wind tend to increase the electron's kinetic energy if it is below $1/2\ Mv_d^2$.

The shape of a cloud of electrons in this frame is, of course, the same as in the laboratory frame. Its main drift velocity is perpendicular to both the magnetic field and the gas wind and is caused by the interaction between the electrons and the gas wind--as explained above for a single electron. Furthermore, it is apparent that elastic collisions with the neutral gas tend to heat the electron cloud to an average (thermal) energy of $1/2\ Mv_d^2$. (This is not as obvious in the laboratory frame.) The inelastic collisions, however, limit the mean electron energy to some value lower than $1/2\ Mv_d^2$.

The drift velocities of the electron cloud can also be easily understood from a macroscopic viewpoint. The gas wind can be considered to exert a force $\vec{F}$ in the $-\vec{v}_d$ direction on the electron cloud by means of its collisions with the cloud. This force gives rise to a drift velocity according to the relationship

$$\vec{v}_E = c \frac{\vec{F}}{Nq} \times \frac{\vec{B}}{B^2}$$

where in this case $q = -e$. Due to this primary drift there is a small Hall effect drift in the $\vec{v}_E \times \vec{B}$ direction. One can carry the argument a step further by noting that $\vec{F}/N$ is the average momentum transfer per electron per unit time, which is of order $m(-\vec{v}_d)$ times ν_c. Thus $\vec{v}_E$ is of order $(\vec{B}/B) \times (-\vec{v}_d)/\omega_b\tau$.

In this frame the electron velocity distribution function is much more nearly isotropic than in the laboratory frame because the largest drift velocity, $\vec{v}_d$, has been transformed away. The main deviation from isotropy is now due to the much smaller drift velocity $\vec{v}_E$. Furthermore, since the speed of each electron is constant between collisions and is changed only because of collisions, the Boltzmann equation to lowest order becomes simply

$$\frac{\partial f^0(v',t)}{\partial t} = \left(\frac{\partial f^0}{\partial t}\right)_{coll} \qquad \text{(II-38)}$$

where it is understood that here f^0 refers to the isotropic part of the electron velocity distribution function in the drift frame and v' is the electron's speed in the drift frame.

After $f^0(v',t)$ attains the form $f^0(v') \exp(\beta t)$, its change with time is due only to the ionization collisions represented by the exponential factor. The ionization rate β is, of course, the same in either frame. Then by Eq. (II-38) the value of $f^0(v')$ at any v' is determined by a balance between the rate at which electrons are scattered from that speed and the rate at which they are scattered to it by all of the collisions. In other words, $f^0(v')$ is determined only by the relative rates (over the whole range of v') of all the various types of collisions. The parametric dependence of $f^0(v')$ is now apparent. There is no electric field in this frame, and the magnetic field does not affect any of the collision rates; therefore $f^0(v')$ does not depend on E or B. All the collision rates are simply directly proportional to the gas density, so a change in n_g does not

affect the relative rates of the various types of collisions; therefore $f^0(v')$ does not depend on n_g. Finally, $f^0(v')$ does depend on v_d because each collision rate depends in a different manner on the relative velocity $\vec{v}' + \vec{v}_d$ between the colliding particles. Thus, the electron speed distribution function in the drift frame depends only upon v_d (and v') for a given gas.

It follows that in the drift frame β/n_g depends only on v_d. In the drift frame the expression corresponding to Eq. (II-14) is

$$\beta = 4\pi n_g \int \sigma_i(\vec{v}' + \vec{v}_d)|\vec{v}' + \vec{v}_d|(v')^2 f^0(v')dv', \qquad \text{(II-39)}$$

and since $f^0(v')$ depends only on v' and v_d it is clear that β/n_g depends only on v_d. This result for the functional dependence of β/n_g also holds in the laboratory frame, for β/n_g is a qunatity which is independent of the reference frame. Furthermore, insofar as the higher order terms in Eq. (II-5) can be neglected so that Eq. (II-14) is a good approximation for β in the laboratory frame, Eq. (II-15) then follows. (Note that Eq. (II-39) is more accurate than Eq. (II-14) because the distribution function is more nearly isotropic in the drift frame.)

III. APPARATUS AND PROCEDURE

A. The Apparatus

The electrodes were of cylindrical geometry and were mounted coaxially on a Lucite base, as is shown in Fig. 8. The base and its brass center piece performed the function of aligning the electrodes with respect to each other and with respect to the magnetic field. The whole electrode structure was located in a vacuum system between the poles of a large magnet.

The anode was a copper cylindrical shell having an inside diameter of 16.5 cm and a height of 8.5 cm. A rectangular array of small holes through the anode, centered with respect to the height of the anode, provided a "window" through which the cathode was illuminated with ultraviolet light. This "window" was about 1 cm high and 3 cm long.

The cathodes were a set of interchangeable aluminum cylinders of different diameters, for the electrode gap spacing was varied by changing to a different cathode. Gap spacings of 0.3, 0.5, and 0.8 cm were employed.

The experimental (or breakdown) region, henceforth called simply "the gap", was the annular space between the two electrodes. Particular attention was paid to the ends of the gap in an attempt to maintain the orthogonality of $\vec{E}$ and $\vec{B}$ everywhere within the gap. Figure 9 shows the details of the construction of the electrode structure at the ends of the gap.

The end insulators were soft glass. They had a thickness of 0.3 cm, and a different pair was required for each different electrode gap spacing. On the side of the glass facing the gap, but in the shadow of the electrodes, conducting layers of silver were painted on the glass. Each of these conductors was electrically connected to the appropriate electrode, although these connections are not shown in Fig. 9. (In this figure the thickness of the silver paint and of the resistance paint and also the distance between the glass and the electrodes are exaggerated for clarity.) The purpose of these painted

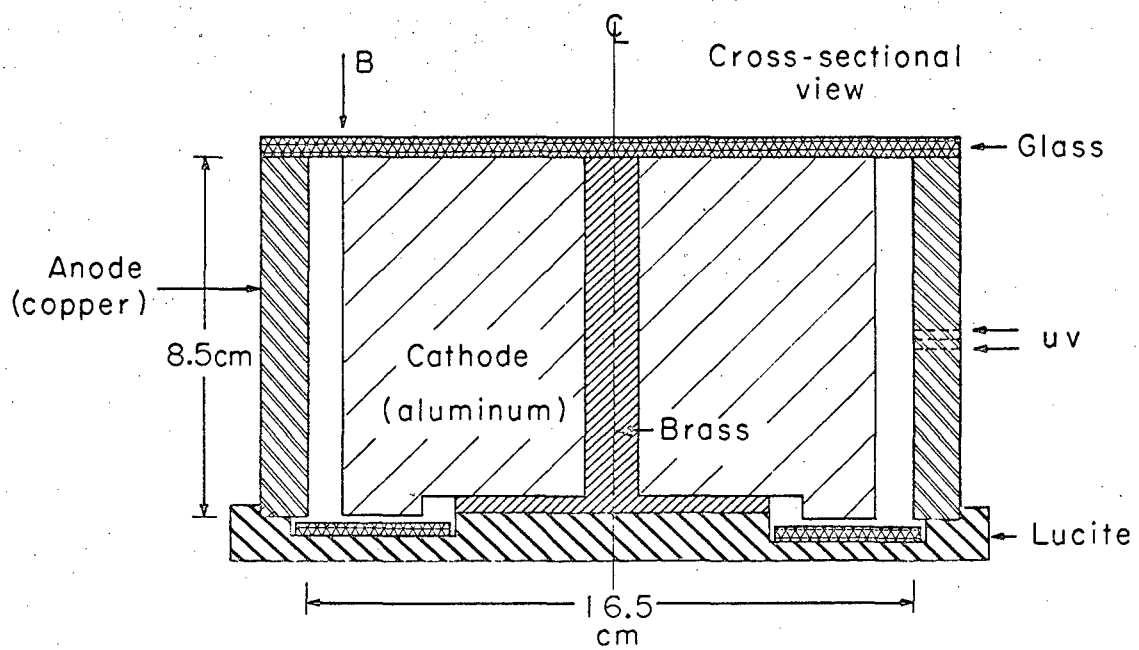

Fig. 8. Schematic drawing of a cross-sectional view of the electrode structure. All parts have cylindrical symmetry about the center.

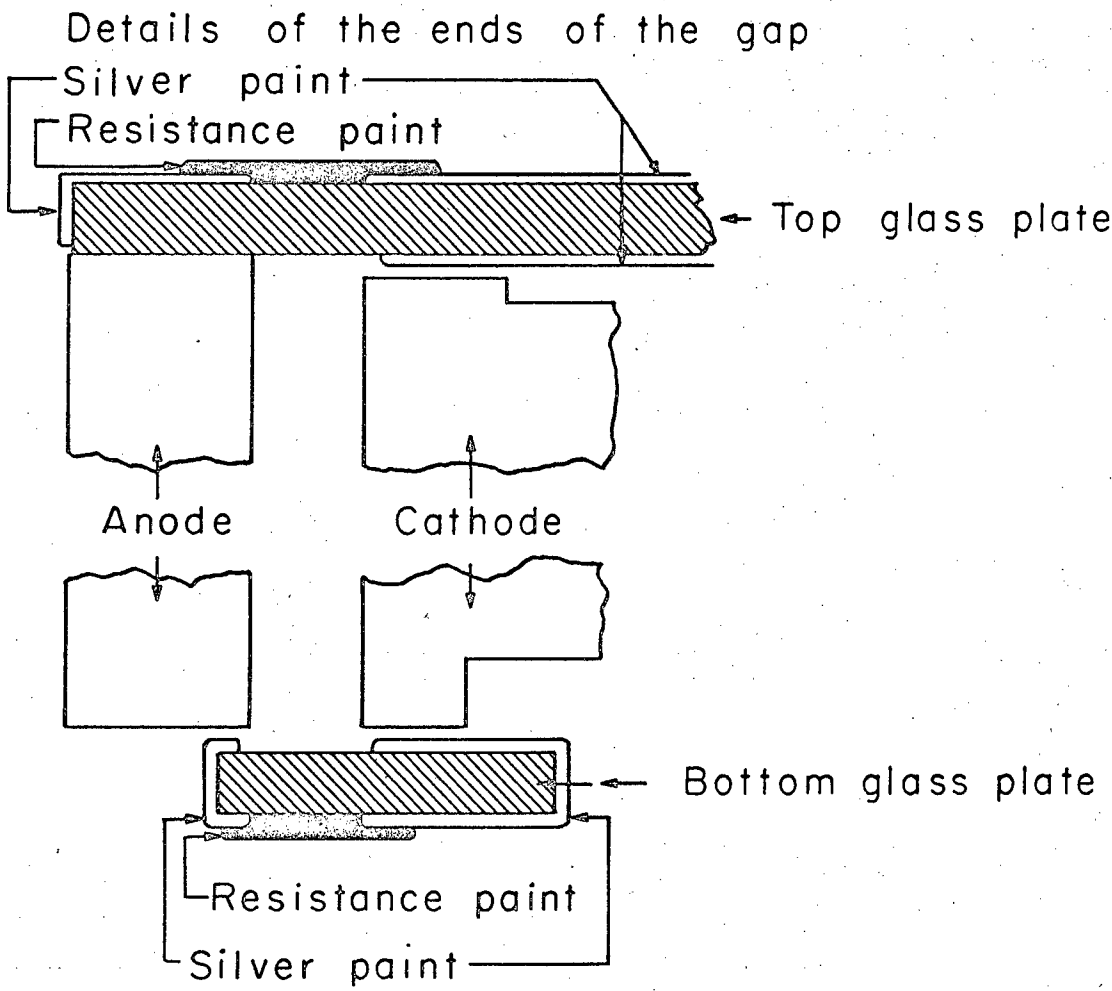

MUB-12988

Fig. 9. Schematic drawing of the details of the ends of the gap. The insulating electrode support and polyethylene insulator which rests above the top glass plate are not shown. The electrical connections between the electrodes and the silver paint are also not shown.

conductors was to collect between breakdown initiations any charge that might have been left on the glass insulator from the previous discharge. The soft glass insulators alone gave much better shot-to-shot reproducibility of the formative time than did Lucite end insulators, but for best reproducibility the silver paint was necessary also.

On the side of the glass end insulators that lay outside of the gap the projection of the electrodes was painted onto the glass with conducting silver paint, as shown in Fig. 9. When this silver paint was electrically connected to the electrodes its effect was to extend the gap geometry to the outside of the insulator. After the silver paint was applied, resistance paint of the printed circuit type was put across the simulated gap on the outside of the insulators. The resistance paint was sprayed onto the insulator as it was turning in a lathe. A layer of insulating lacquer applied over the resistance paint is not shown in Fig. 9.

The purpose of the "end resistors" on the outside of the end insulators was to grade the potential uniformly across the gap and thus simulate a gap of infinite length. In other words, they were to force the equipotential lines to run straight out of the gap so that the end effects did not appear in the experimental region. There was, of course, some distortion due to the fact that these end resistors were on the other side of the insulators from the actual ends of the gap, but it was deemed advisable to keep the resistance paint out of the discharge region.

Actual measurements of the uniformity of the potential across the end resistors were not attempted. However, when the voltage across test resistors in air was increased until high voltage breakdown across the resistor occurred, it was always found that the breakdown had occurred through the air over the resistor and not through the resistance paint itself. Even when insulating lacquer was painted over the resistance paint and the silver paint this same result was obtained. The spark would go up through the lacquer, through the air, and back down through the lacquer to the other side of the resistor.

These tests seem to indicate that the resistance paint did a remarkable job of grading the potential uniformly.

The shunt resistor composed of the two end resistors in parallel is labeled R_g in Fig. 12. The value of R_g was determined by two considerations. First, in order that the end resistors could perform their intended function before the avalanche growth was well underway, $C_e R_g$ had to be less than the voltage risetime (0.1 μsec), where C_e is the capacity to the grounded "field-shaping" steel plates (see Fig. 10). For a 1.0 cm electrode gap spacing C_e was estimated to be about 10 pF. Second, in order that R_g not significantly drop the magnitude of the potential across the electrodes during the avalanche growth, $R_g C_0$ had to be very long compared to the observed formative times. The (high voltage) values of R_g that were desired ranged from 10 kΩ to 40 kΩ depending on the electrode gap spacing. However, the actual construction of the end resistors was somewhat tricky, and it was found to be rather difficult to end up within even a factor of two of any desired resistance. One of the difficulties was that for a given electrode gap spacing the value of R_g was a function of the applied voltage V_g. (The high voltage values of R_g were measured in air by observing the RC decay time when a capacitor was discharged through the combination of R_g and a known smaller resistor in parallel with it.) The value of R_g for a V_g corresponding to an E of 5 or 6 kV/cm was generally found to be one-third to one-tenth of the value of R_g for a V_g of a couple of volts. Although the value of R_g varied significantly over the experimental range of V_g, the effect caused no concern because for the higher values of V_g the formative times were shorter so that a lower value of R_g was actually desirable.

The magnetic field was provided by a large electromagnet having 18 in. by 36 in. rectangular pole faces. An aluminum vacuum chamber was inserted into the 8-in. gap between the magnet poles. Within the vacuum chamber were two precision-ground 1-in. thick circular flat steel plates, henceforth called the "field-shaping" plates, whose function was to provide a more uniform magnetic field in the experimental region. The magnet, the vacuum tank, and the "field-shaping"

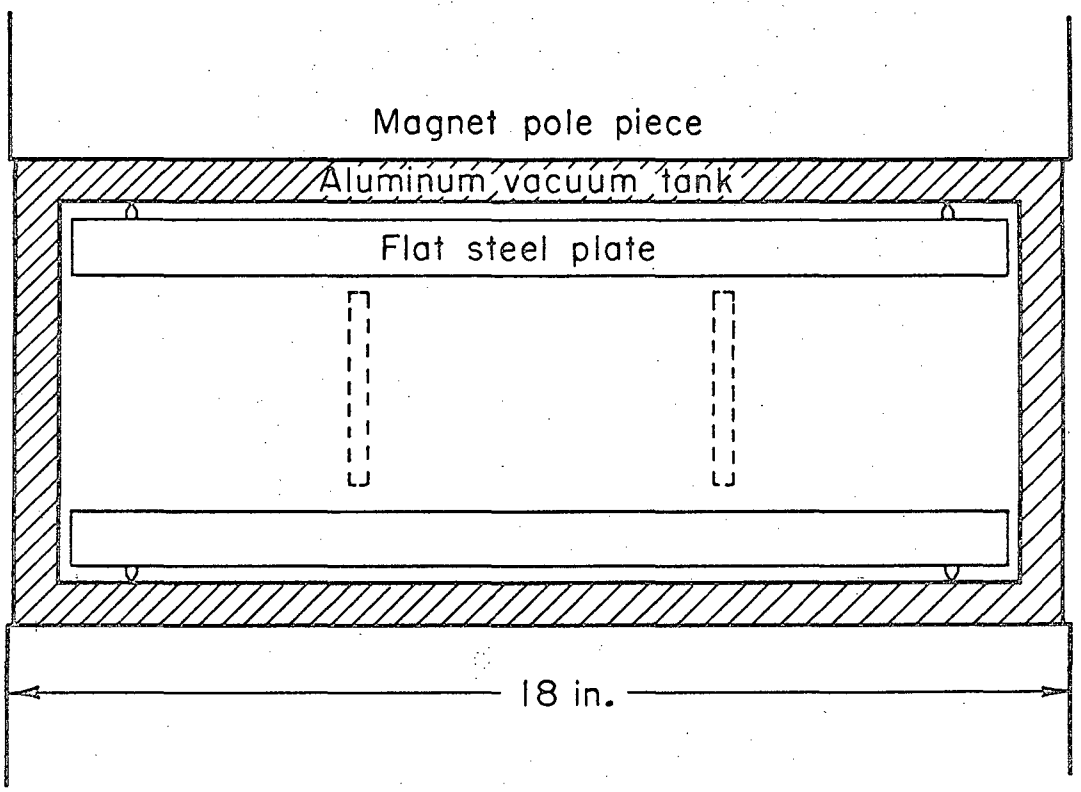

XBL673-2450

Fig. 10. Scale drawing of a cross-sectional view of the vacuum tank and the "field-shaping" steel plates. The dotted rectangles show the position of the electrode gap.

plates are shown in Fig. 10, which illustrates a cross-sectional cut through the narrow dimension of the magnet pole pieces. The two "field-shaping" plates were mounted together parallel to each other to form a single unit by four spacers (not shown in Fig. 10). The electrode structure was placed directly on the bottom steel plate.

The magnitude of the magnetic field was calibrated by a rotating-coil gaussmeter. A Hall probe was used to set the level of the magnetic field while taking data. The uniformity of the magnitude of the magnetic field over the experimental region was checked by a search coil connected to an electronic integrator. The field was found to be constant within 0.02% at 12 kG and within 0.25% at 19 kG. The range of the magnetic field that was used in the experiment was $6\ \text{kG} \leq B \leq 18\ \text{kG}$.

The vacuum chamber consisted of a large (about 185 liters) aluminum tank with two Lucite windows and several brass flanges. Rubber O rings and gaskets were used to seal the many joints. A 14-in. oil diffusion pump provided a base pressure of (2 to 3) x 10^{-7} torr. The occasional use of a liquid-nitrogen cold-trap inserted into the vacuum chamber resulted in a decrease in the base pressure of about a factor of two. The diffusion pump was isolated from the rest of the vacuum system before the hydrogen was admitted into the system at the beginning of an operating period. During the operation of the experiment the liquid-nitrogen cold-trap was used to pump the condensable impurities, although no effect on the data was detected if it was not used. The experiment was operated with static gas conditions, for no difference in the data was observed between this manner of operation and the case where there was a slow continuous gas flow.

The gas pressure was measured with an oil manometer to an accuracy of about 5 x 10^{-3} torr. There was no detectable change in the gas pressure due to operation of the experiment. The range of gas pressures used in the experiment was $0.2\ \text{torr} \leq p \leq 2.0\ \text{torr}$. The upper limit was set by the condition that the observed formative time be at least about equal to the risetime of the potential across the gap. The lower limit of the pressure range was determined by the electron diffusion along the magnetic field according to the criterion that a typical electron make an ionizing collision before it is lost

by diffusion. This matter is discussed in Section V D.

A quartz lens was mounted in one of the Lucite windows of the vacuum chamber so that ultraviolet light from a germicidal mercury lamp could be focused through the anode "window" onto the cathode. (Because of the large fringe field of the magnet, it was necessary to place the mercury lamp outside of the vacuum system about 1.5 m away from the cathode.) The presence of the end resistors (the resistance paint in Fig. 9 and R_g in Fig. 12) connected electrically across the gap rendered impossible a measurement of the photoelectric current I_0. For the 0.8 cm gap (and also for a 1.0 cm gap) there was no difference in the magnitude of the formative time and very little difference in the shot-to-shot reproducibility of the formative time depending on whether or not the mercury lamp was on. For the 0.5 cm gap and the 0.3 cm gap, however, when the mercury lamp was off the shot-to-shot reproducibility was very poor; but when the lamp was turned on the observed formative times collapsed into a much smaller range of values located at the minimum of the range of values that had been observed when the lamp was off. Figure 11, which shows copies of typical oscilloscope traces of the gap voltage as a function of time, illustrates the sort of shot-to-shot reproducibility that was obtained.

The discharge circuit is shown in Fig. 12. The power supply charged the main capacitor C_0 to a voltage V_0, and upon firing the 5C22 thyratron this voltage appeared across the gap and its shunt resistor R_g. The electrode construction dictated that the anode (outer electrode) be grounded; therefore negative voltage was pulsed onto the cathode. The voltage V_0 was measured with a precision dc voltmeter. A 20 kΩ to 50 Ω voltage divider was used to measure the gap voltage V_g. The voltage measuring circuit was not connected directly across the electrodes. Instead it was placed at a more convenient spot outside of the vacuum system. There were 4 ft of cable between the electrodes and the measuring circuit.

The function of the series resistor R was to limit the energy dissipated in the gap. Since the risetime of the potential across the electrodes was limited by the charging time of the cable capacitance

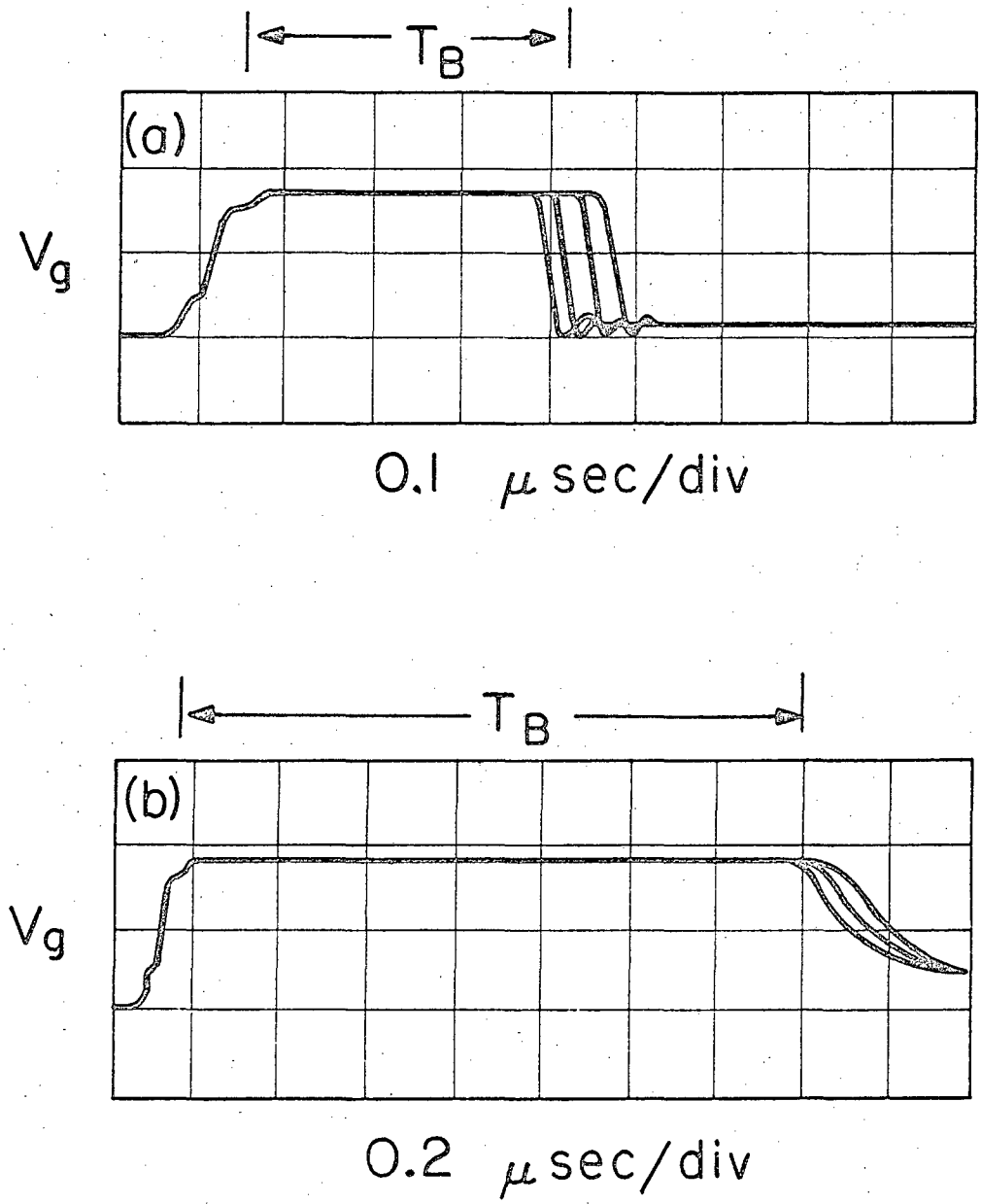

XBL673-2408

Fig. 11. Typical oscilloscope traces of the potential across the electrodes as a function of time. (a) 0.8 cm gap; 1.0 torr; 7.2 kV; 18 kG (four trace overlay). (b) 0.8 cm gap; 1.0 torr; 3.6 kV; 18 kG (five trace overlay).

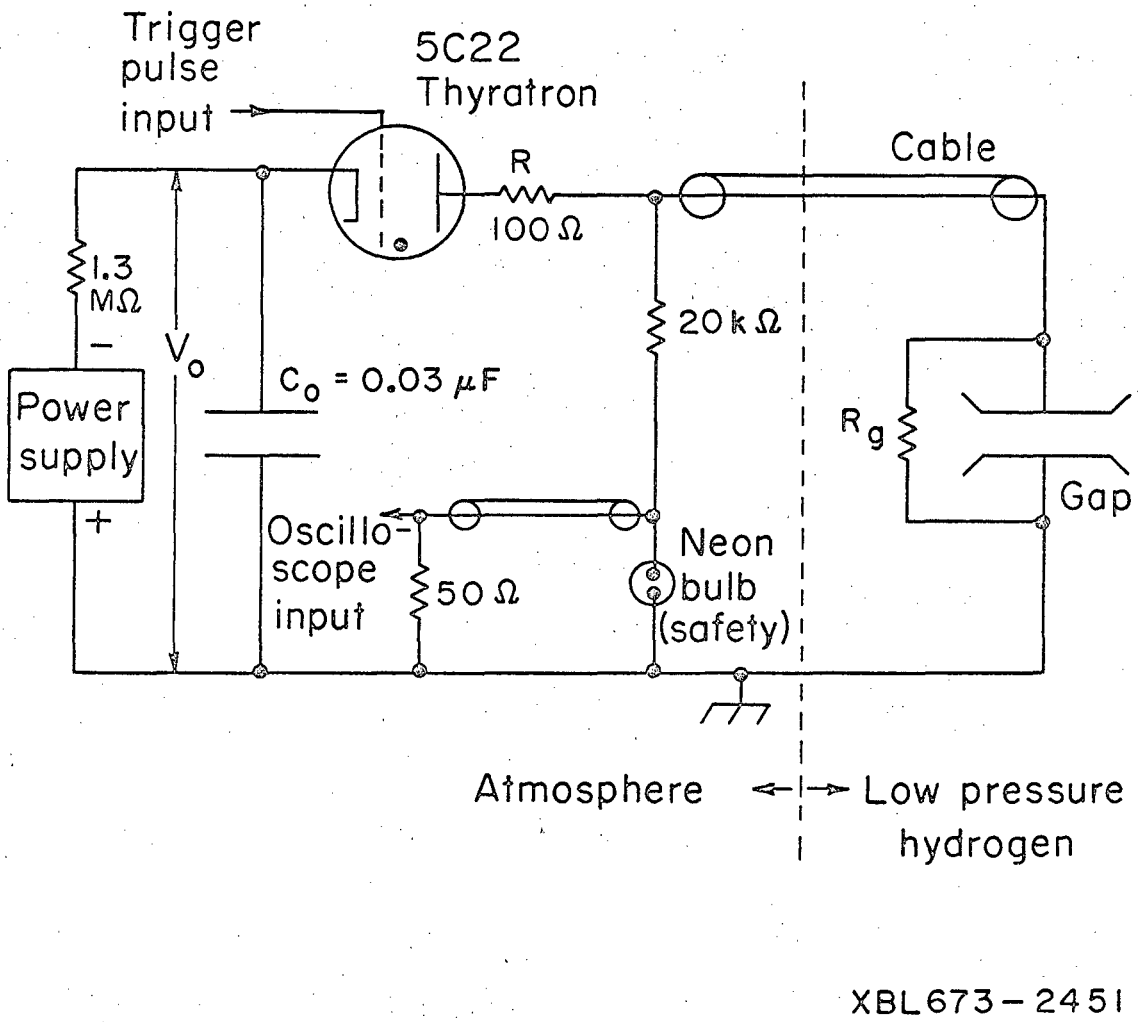

Fig. 12. Diagram of the electrical circuit.

and the electrode capacitance, it was desirable that the value of R be kept small. On the other hand, R also performed the function of damping an undesirable oscillation in the circuit that was due to charge sloshing back and forth between C_0 and the electrode capacity. These considerations dictated the values of 100 Ω for R.

B. The Procedure

As has been previously described, the vacuum chamber was filled with hydrogen to a pressure measured by a manometer and the magnetic field was set with the use of a Hall probe and the voltage across the main capacitor C_0 was adjusted to give the desired electric field. Then four or five pictures of the oscilloscope trace of the voltage across the electrodes as a function of time were taken in superposition. The interval of time between successive breakdown initiations was 10 sec. Figure 11 shows two examples of copies of typical pictures thus obtained.

When the experimental parameters (p, B, and E) were set such that primary avalanche breakdown was expected, no extensive "conditioning" of the gap was necessary before taking data. A first shot established the beginning of the first 10-sec interval, and the following shots were recorded. The interval of time between successive shots, however, did have an effect on the observed formative time. In general, if one shot rather quickly, say once every half second, the average formative time tended to be less and the shot-to-shot scatter tended to be less than if one shot slowly, say once every 30 sec. Although this effect was minimized by the end geometry described previously, it was never completely eliminated. As mentioned above, the interval used was 10 sec between shots. The systematic difference between the average formative time with a 10 sec interval and that obtained with a 1/2 sec interval was of the order of 5% (or less). Usually, but not always, the shorter interval resulted in a shorter formative time. The difference between a 10 sec interval and a 5 sec interval was usually not detectable in a small number of shots because of the scatter.

The above remarks about the effect of the time interval between breakdown initiations apply to primary avalanche conditions only. In general, more shot-to-shot scatter and also a greater sensitivity to the interval between shots were observed if the experimental parameters were such that multiple avalanche breakdown was expected.

As can be seen in Fig. 11, V_g did not rise smoothly to its full value. Instead there were two bumps in the rising voltage as seen by the voltage measuring circuit. These two exactly reproducible bumps were due to reflections of the rising voltage signal from the electrodes. (Naturally there were corresponding but earlier perturbations in the actual voltage across the gap.) The center of the second bump on the voltage trace, which occurred at about 85% of full voltage, was arbitrarily chosen as the zero point of time in the measurement of the formative time from the voltage traces. The end of the formative time was chosen to be at the beginning of the observable drop in the trace. In cases such as the four-trace overlay in Fig. 11 this definition of the end of the formative time presented no problems. In cases such as the five-trace overlay in Fig. 11, however, there was admittedly a little judgment involved.

IV. RESULTS

A. 1/p Dependence of T_B

According to Eq. (II-30), which is assumed to be valid for primary avalanche breakdown, the formative time should be inversely proportional to the pressure at constant E and B. Figure 13 shows an example of the measured formative time plotted against the reciprocal of the gas pressure. This figure illustrates a case where the formative time T_B was considerably less than the time T_c required for a single electron to drift across the electrode gap, so here the breakdown was of the primary avalanche type. (T_c is obtained from Eq. (II-21) which was obtained from an extrapolation of the drift velocity measurements of Bernstein.) It is seen that the predicted pressure dependence was indeed observed.

Figure 14 shows another example of the measured formative time as a function of 1/p, but for a case where $T_B \approx T_c$. It is seen that in this particular case the formative time varied somewhat from a linear dependence on 1/p. (In other cases where $T_B \approx T_c$ the linear dependence was observed.) It is also evident that for the conditions of this figure there was considerably more scatter in the formative times at the lower gas pressures than at the higher pressures. This behavior was typical for all of the data whenever the magnitude of the formative time at low pressures exceeded a few microseconds. Both this tendency towards greater scatter at the lower pressures and the deviation from linearity with 1/p in Fig. 14 can be ascribed to electron losses by diffusion along the magnetic field to the end insulators, as is discussed in Section VD.

Figure 15 shows an example of the observed formative time as a function of 1/p for a multiple avalanche case. The nonlinear dependence of T_B on 1/p illustrated in this figure was typical of the observations in the multiple avalanche regime. Some of the deviation at low pressures was undoubtedly due to electron losses along the magnetic field.

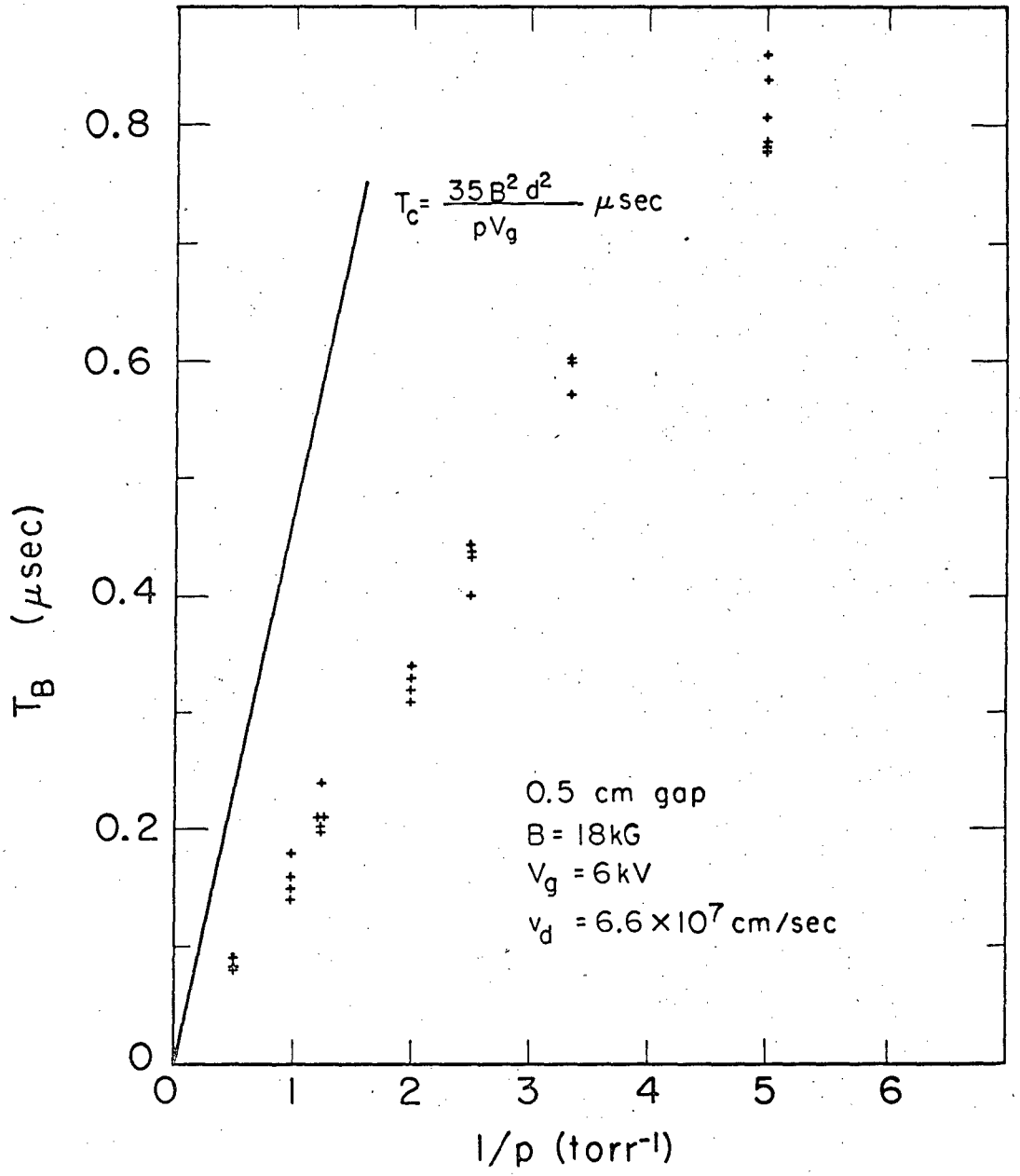

XBL673-2409

Fig. 13. The formative time as a function of 1/p for a case where $T_B < T_c$. Each point represents a single shot.

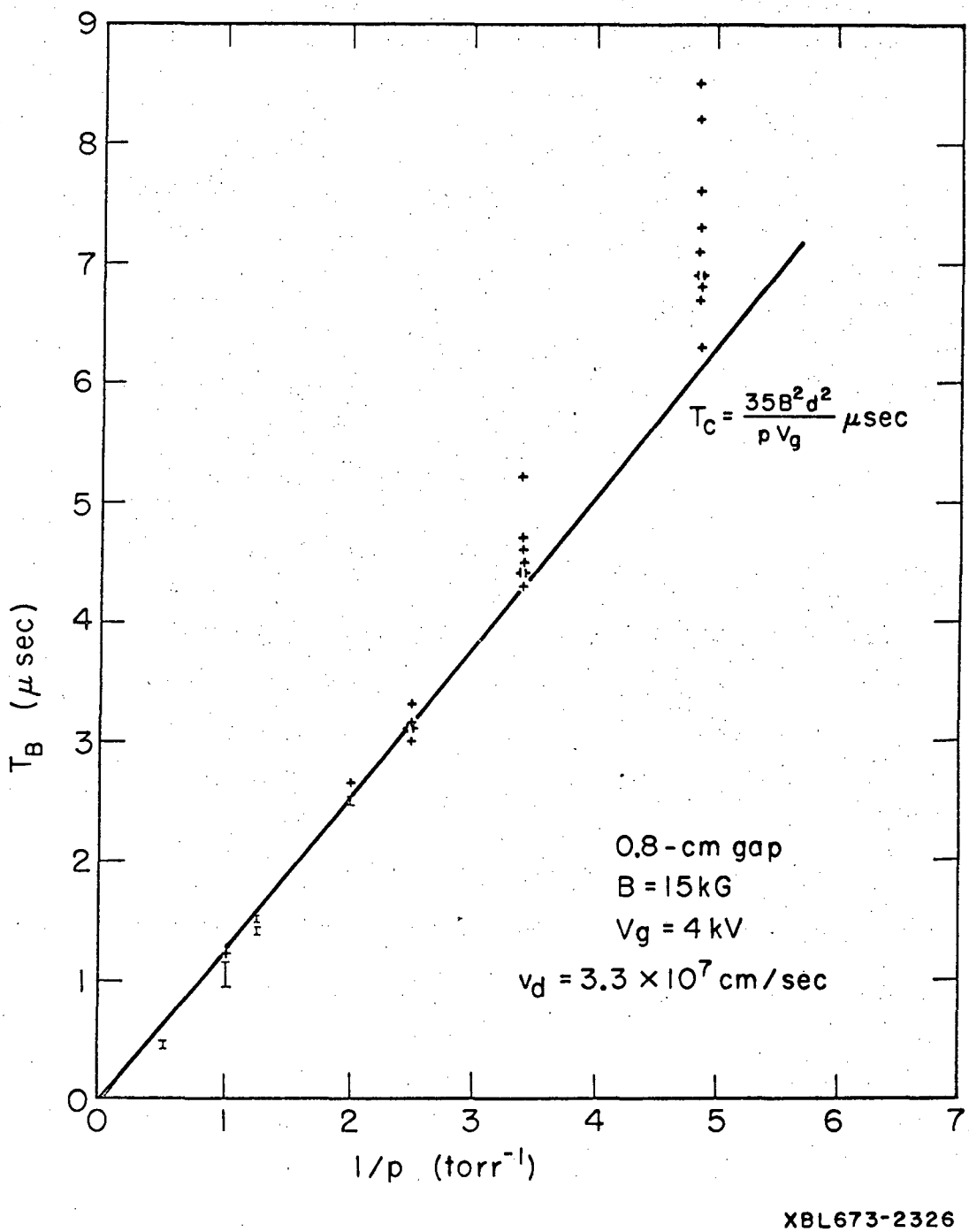

Fig. 14. The formative time as a function of 1/p for a case where $T_B \approx T_c$. The crosses represent single shots, and the bars represent a group of several shots.

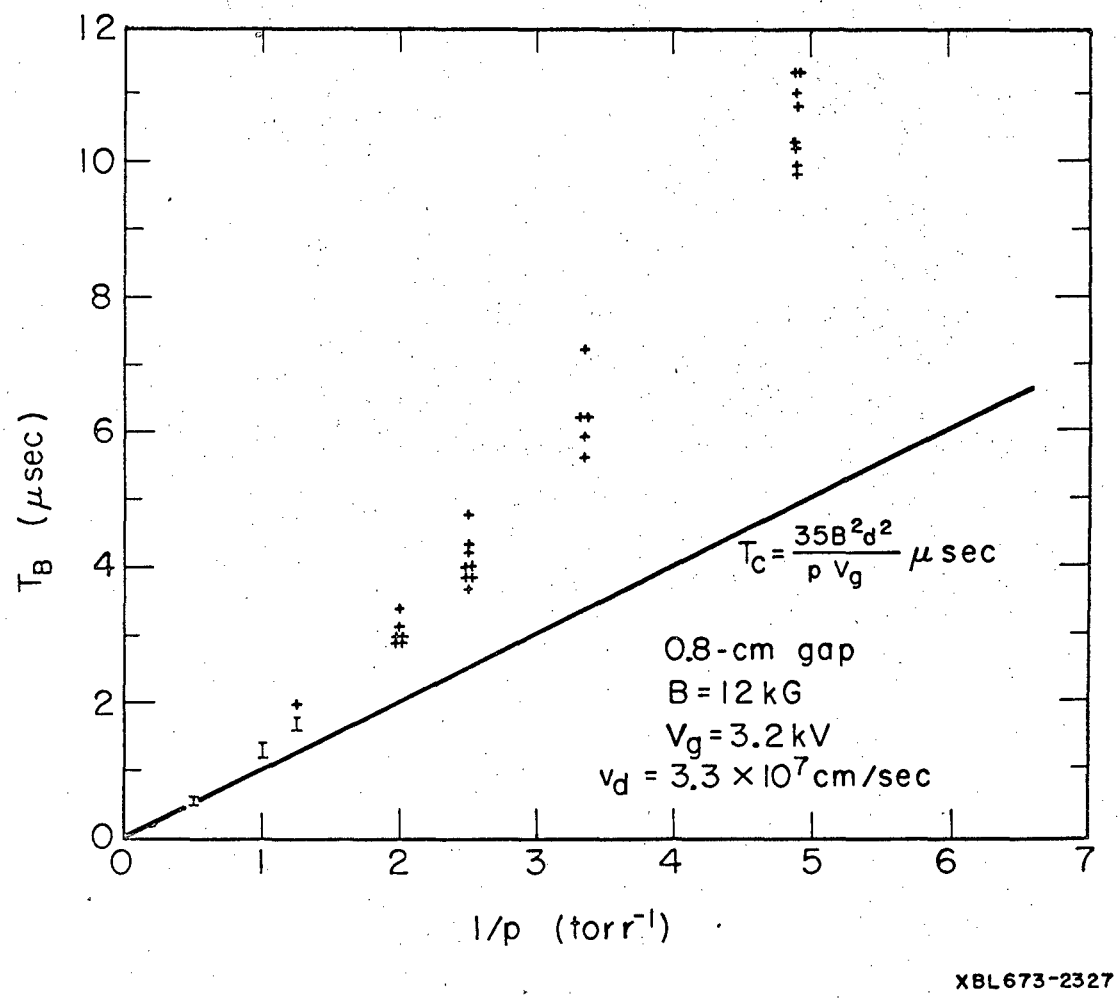

Fig. 15. The formative time as a function of 1/p for a case where $T_B > T_c$. The crosses represent single shots, and the bars represent a group of several shots.

The experimental results for the dependence of the formative time on the pressure can be summarized as follows: The linear dependence of the formative time on the inverse pressure was always observed when the fields were such that the breakdown was well into the primary avalanche regime, and the linear dependence was not observed when the breakdown was well into the multiple avalanche regime. For field conditions such that $T_B \approx T_c$ the linear dependence was usually observed, but there were exceptions such as illustrated by Fig. 14.

Although the 1/p dependence of T_B is admittedly not a sensitive means of distinguishing between single and multiple avalanche breakdown in the transition region, the author is tempted to guess (on the basis of some cases where the linear dependence of T_B on 1/p was found when T_B was slightly larger than T_c) that the expression for T_c as given by Eq. (II-21) is too low. This would indicate that v_E in the range of v_d of this experiment is less than the value measured by Bernstein at $v_d = 7 \times 10^6$ cm/sec.

B. E/B Functional Dependence of $n_g T_B$

According to the arguments of Section II, the product of the formative time and the gas pressure depends only on the ratio of the electric field to the magnetic field and not on either field separately. In Figs. 16 through 19 the product $n_g T_B$ at constant E/B is plotted against B for comparison with this theoretical prediction. Figure 16 shows the data for the 0.8 cm gap alone at three values of v_d. In Figs. 17 through 19 the data for each drift velocity are shown separately, including the results for all values of the electrode gap spacing. Each of the data "points" in these four figures was obtained from the slope of a straight line drawn through the data of a pressure dependence graph such as illustrated in Figs. 13 through 15. The length of the data bars in Figs. 16 through 19 represents the uncertainties in determining these slopes. Those cases where the formative time was greater than T_c as given by Eq. (II-21) are denoted by the small letter m.

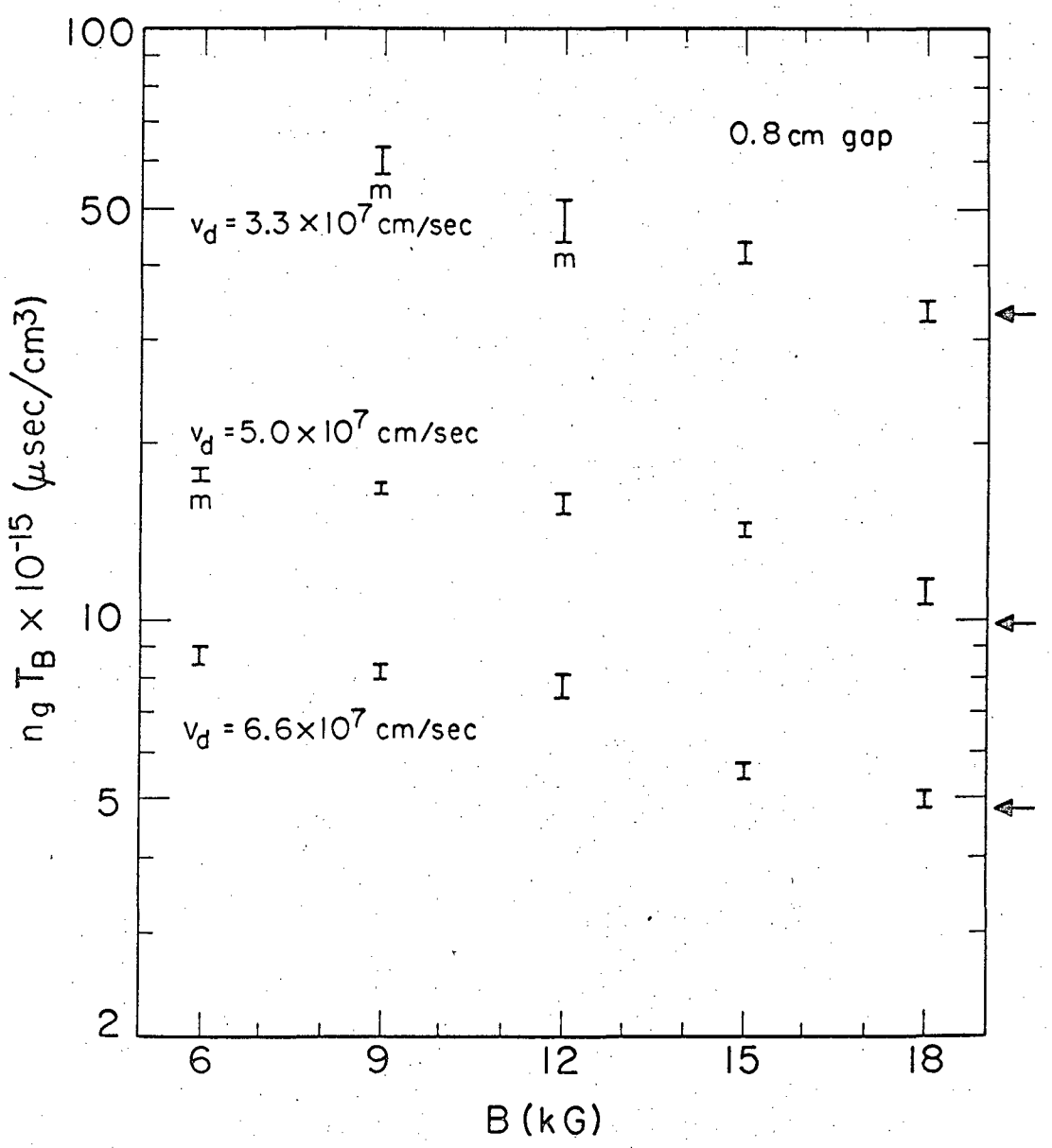

Fig. 16. The product of the measured formative time and the gas density plotted against the magnetic field strength for the 0.8 cm gap. The data labeled with the letter m are cases where $T_B > T_c$.

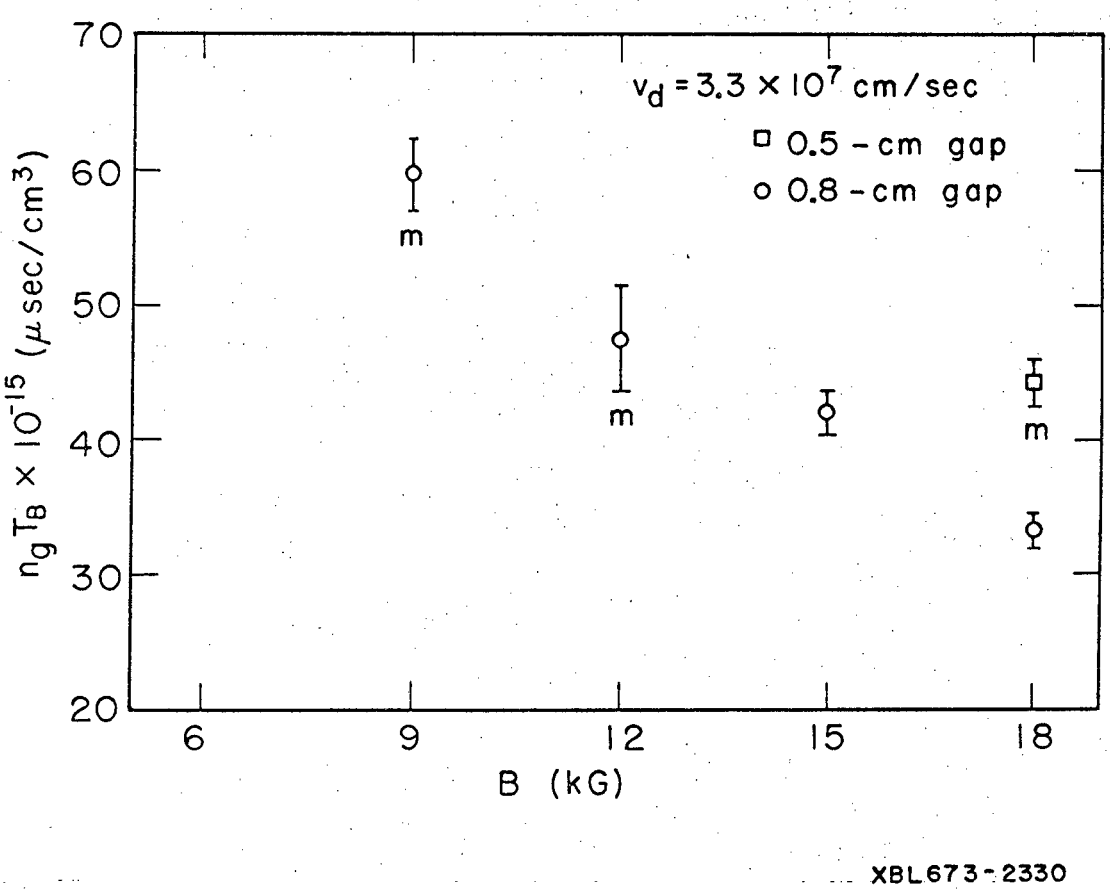

Fig. 17. The product of the measured formative time and the gas density for $v_d = 3.3 \times 10^7$ cm/sec. The data labeled with the letter m are cases where $T_B > T_c$.

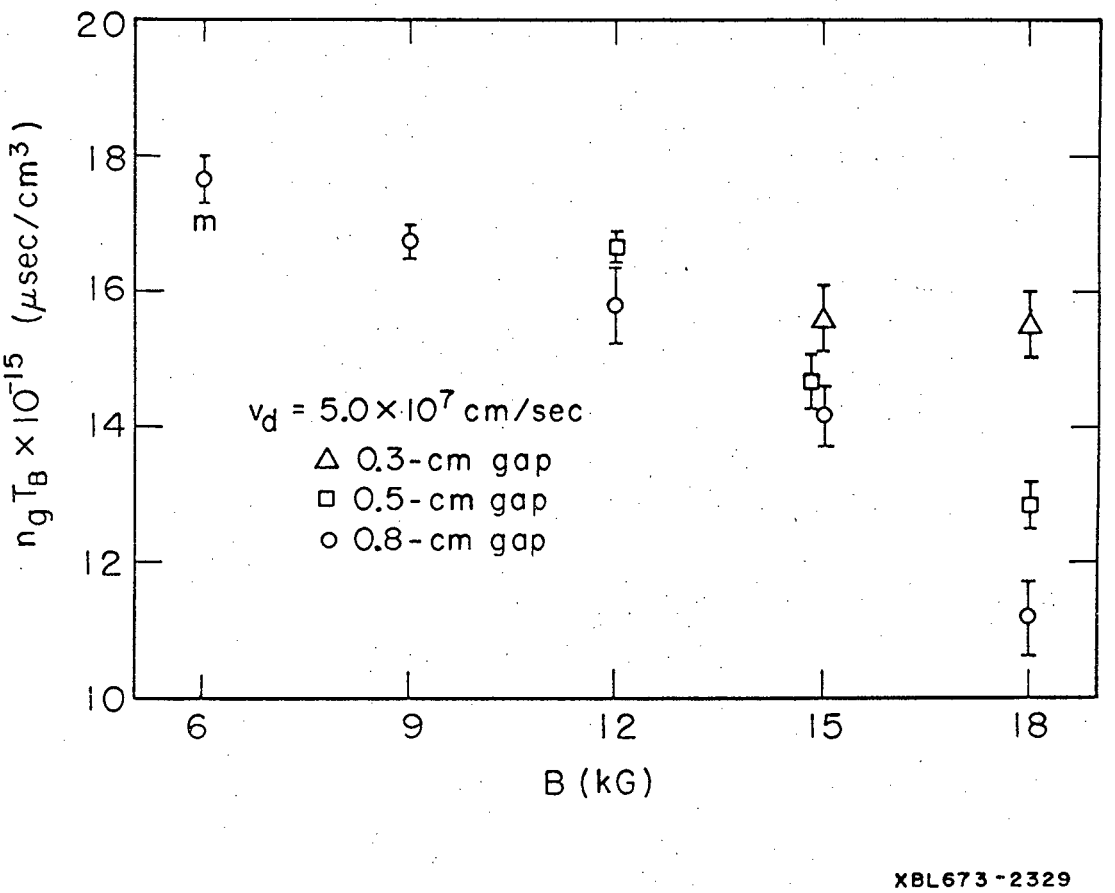

Fig. 18. The product of the measured formative time and the gas density for $v_d = 5.0 \times 10^7$ cm/sec. The data labeled with the letter m are cases where $T_B > T_c$.

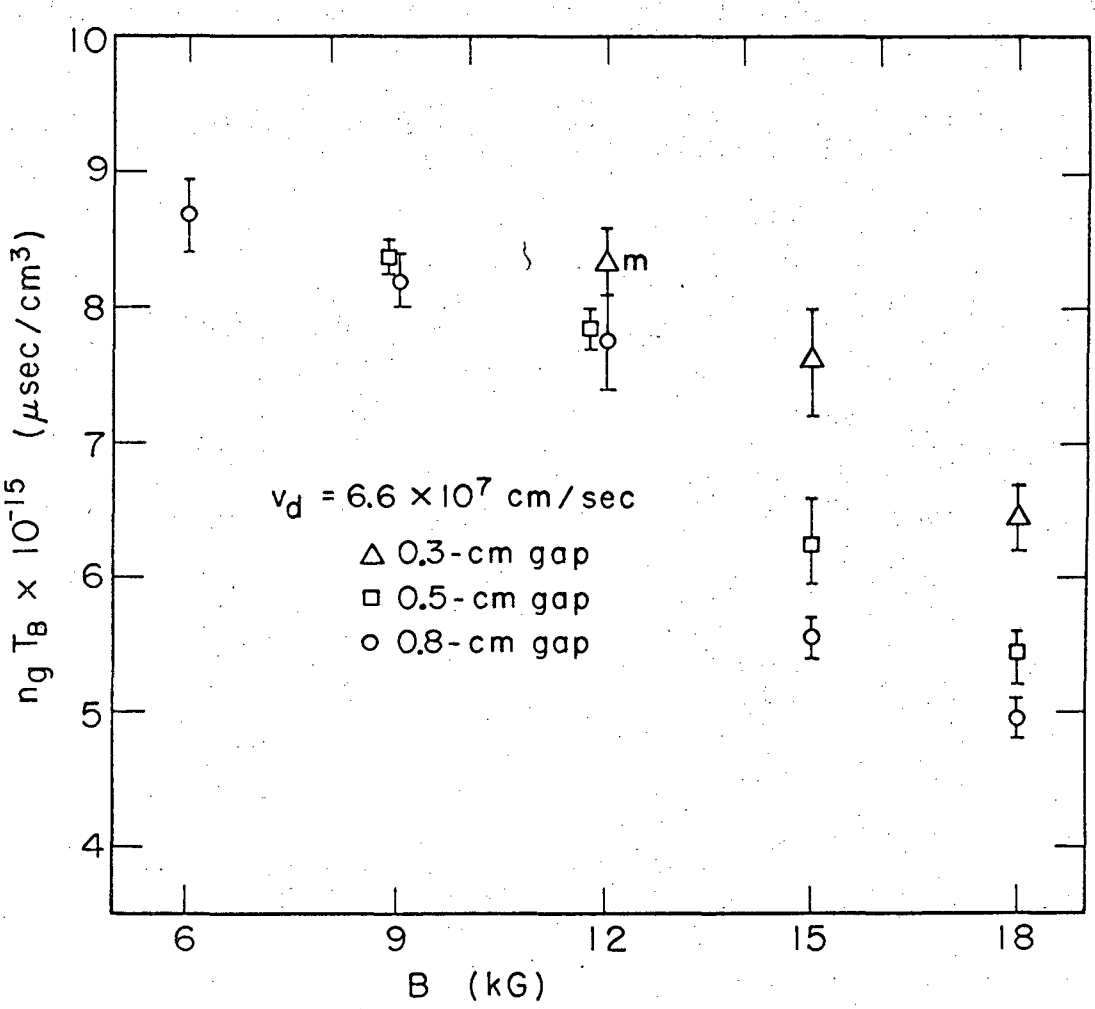

Fig. 19. The product of the measured formative time and the gas density for $v_d = 6.6 \times 10^7$ cm/sec. The data labeled with the letter m are cases where $T_B > T_c$.

It is immediately evident from these graphs that some deviation from the prediction of Eq. (II-30) concerning the functional dependence of the formative time on the ratio E/B (or v_d) was observed. The product $n_g T_B$ was found to decrease with increasing B (or E) at constant E/B.

It is also of interest to note that there was no sharp change in the magnitude of the observed formative time as the breakdown conditions passed from the single avalanche regime into the multiple avalanche regime. Such a change is expected in the simple model of Section II because when $T_B > T_c$ the primary avalanche gets quenched at the anode causing the breakdown to be delayed until the weaker secondary electron effects--see Section VB and Appendix C--can build up sufficiently. The fact that this expected sharp change was not observed may indicate that, at least when the field magnitudes were such that $T_B \approx T_c$, secondary electron effects were indeed important (contrary to the discussion of Section VB).

From Figs. 18 and 19 it is evident that the size of the electrode gap had an effect on the observed formative time and that the effect increased with increasing B (or E) at constant E/B. This effect is not predicted by the model of Section II; and it is not understood. Qualitatively, the decrease in the effective gap size with increasing magnetic field because of the bowing of the magnetic field lines (see Section VA and Fig. 20) combined with the primary electron losses at the anode that occur when the initial electrons are distributed throughout the gap (see Section VC) would be expected to produce such an effect. (The percentage decrease of the gap would be larger for a smaller gap width, so that for it the increased electron losses at the anode would be more important than for a larger gap width.) But the extent of the bowing of a magnetic field line is so small (5×10^{-3} cm) compared to the gap widths that this cannot be the explanation.

C. Magnitude of $n_g T_B$

In this section the magnitudes of the measurements of the formative time are compared with the predictions of Section II. The

predictions are based on the five estimates for the ionization frequency β (Fig. 5) and the assumption that βT_B equals a constant independent of the gas pressure and the applied fields. The data for the 0.8 cm gap at 18 kG are used for this comparison under the assumption that for this case the electron losses along the magnetic field (Section VD) are minimized (by the bowing of the magnetic field lines--Section VA) so that the closest agreement with the theory of Section II is expected.

The quantity actually compared is $n_g T_B \times 10^{-15}$ μsec cm^{-3} from Fig. 16. For $\beta T_B = 25.5$

	v_d		
	3.3×10^7 cm/sec	5.0×10^7 cm/sec	6.6×10^7 cm/sec
β curve 1	18	7.3	4.4
β curve 2; Eq. (II-37)	16	6.4	3.5
β curve 3; Eq. (II-35)	21	8.7	5.1
β curve 4	36	11	6.2
β curve 5; Eq. (II-36)	31	9.3	4.6
observed (18 kG)	32-35	10.5-11.5	4.8-5.1

where the β curves are those of Fig. 5. In Section IID it was estimated that βT_B ranged from 25.5 to 27 at the observable voltage collapse. Using $\beta T_B = 27$, the comparison for $n_g T_B$ is

	v_d		
	3.3×10^7 cm/sec	5.0×10^7 cm/sec	6.6×10^7 cm/sec
β curve 1	19	7.8	4.7
β curve 2; Eq. (II-37)	17	6.8	3.7
β curve 3; Eq. (II-35)	22	9.2	5.4
β curve 4	39	12	6.7
β curve 5; Eq. (II-36)	33	9.8	4.8
observed (18 kG)	32-35	10.5-11.5	4.8-5.1

The predictions of β curve 5 and $\beta T_B = 27$ are marked by small arrows on Fig. 16.

It is thus seen that the observed formative times at 18 kG are in good agreement with the predictions based on (1) the experimental measurements for α of Bernstein[6] and Fletcher and Haydon,[17] and (2) the extrapolation of Bernstein's measurement for v_E.

V. DISCUSSION

A. Field Imperfections

A discussion of the effects on the observed formative time of deviations of the electric and magnetic fields from the spatially uniform and mutually perpendicular configuration assumed in Section II is now presented.

If the fields are not mutually perpendicular there is a component of the electric field, $E_{\|}$, in the direction of the magnetic field. Because of $E_{\|}$ the electrons acquire additional energy between collisions with the gas molecules which was not included in the analysis in Section II. This additional energy gain results in additional heating of the electrons and therefore increases the ionization rate. The effect increases with E independently of B and might explain the deviation of the results from Eq. (II-30).

One field configuration with an $E_{\|}$ is the case where the electric and magnetic field lines are essentially straight but are not orthogonal, such as would be expected if the electrode structure were misaligned so that the magnetic field lines were not parallel with the surface of the electrodes. This is a particularly undesirable case because for it all of the electrons are subject to $E_{\|}$ during the whole life of the avalanche. To estimate for this case the upper limit on the acceptable deviation from orthogonality (or equivalently how accurately the electrodes must be aligned with the magnetic field), suppose it is required that the energy an electron gains between collisions from $E_{\|}$ be less than 1/5 of mv_d^2 (which is the average energy gain per collision in a pure $\vec{E} \times \vec{B}$ geometry). Then, as in Section IIB, for $v_d = 6.6 \times 10^7$ cm/sec one can use $4 \times 10^9 p \ \text{sec}^{-1}$ for the collision frequency and $\bar{\epsilon} = 20$ eV to obtain the condition

$$E_{\|} \ (\text{volts/cm}) < 10p \ (\text{torr}).$$

For p = 0.5 torr and E = 10 kV/cm,

$$\theta \equiv \frac{E_{\|}}{E} < \frac{1}{2} \times 10^{-3} \ \text{radian}.$$

Although it was believed that the electrodes were aligned accurately enough, a test for the presence of this effect was performed at a pressure of 0.4 torr by observing the effect on the formative time of a deliberate tilt of the whole electrode structure. The results of this test were:

(1) The formative time was rather insensitive to tilts of 1 to 2×10^{-3} radian.

(2) Once an effect could be detected (around 2 to 3×10^{-3} radian), the formative time decreased monotonically with increasing tilt. At a tilt of 5×10^{-3} radian the formative time had decreased about 15% from its value with no tilt.

It was concluded that misalignment of the electrodes with the magnetic field was not responsible for the deviation of the results from the theory of Section II. The observation that the alignment was not as critical as the previous estimate would indicate was probably due to the slight bowing of the magnetic field lines. The effect of this bowing is discussed next.

Another field configuration with an $E_{\|}$ is the case where the electric field lines are straight but the magnetic field lines are slightly curved. This field configuration was indeed present in the experiment. According to the magnetic field measurements the field intensity at the gap was not quite as high as at the axis of symmetry; therefore the magnetic field lines were slightly bowed outward from the cathode, as shown schematically in Fig. 20. At the higher magnetic fields the amount of this bowing increased as the magnetic field intensity increased because of iron saturation effects. Thus as E and B were increased, keeping E/B constant, the magnitude of $E_{\|}$ grew because of both the increase in E and the increase in the bending of the magnetic field lines.

Nevertheless, the effect of $E_{\|}$ on the formative time is not expected to be as large in this case as in the previously considered case where the fields were uniform but not orthogonal. This is because the symmetrical (about the midplane with respect to the axial direction) bending of the magnetic field lines back towards the cathode

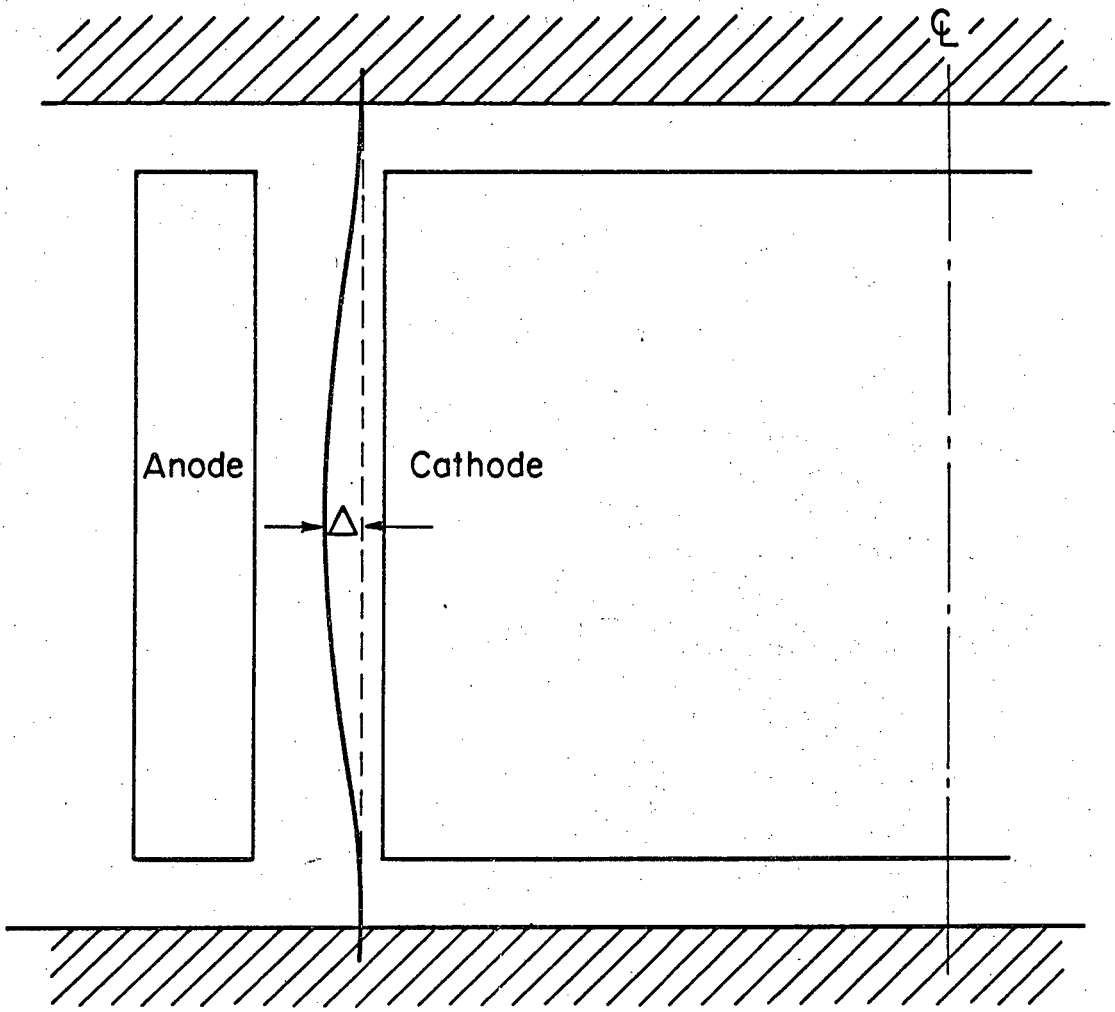

Fig. 20. Schematic diagram of the bowing of a magnetic field line. The line displacement distance Δ is exaggerated.

has the effect of focusing the avalanche toward the midplane, for the motion of the electrons in the axial direction away from the midplane is inhibited by $E_{\|}$. As the avalanche grows this focusing effect will be opposed and then overcome by the net space charge that results from the positive ion removal. So in this geometry the main ionization effect of $E_{\|}$ is expected to occur early in the avalanche growth and to be on the electrons near the ends of the gap. These electrons will be accelerated towards the midplane by $E_{\|}$ and could acquire from it enough "extra energy" (i.e. unaccounted for in the analysis of Section II) for three or four ionizing collisions, as will be shown in the next paragraph. After a few ionizing collision times the avalanche becomes focused and the effect of $E_{\|}$ on the ionization rate diminishes. Therefore the effect of increasing $E_{\|}$ can in this case be approximated by an increase in the effective number of initial electrons, N_0.

The magnitude of this effect can be estimated from the magnetic field uniformity measurements. (See Section IIIA.) According to these measurements the magnetic field at the gap was 0.25% less than at the axis of symmetry when the magnitude was 19 kG. The corresponding figure for 12 kG was less than 0.02%. Using the field profiles obtained from the uniformity measurements, a simple calculation based on the conservation of flux yields the following estimates for the line displacement distance Δ shown in Fig. 20:

$$\Delta \approx 5 \times 10^{-3} \text{ cm} \qquad \text{for 19 kG}$$
$$\Delta \approx 3 \times 10^{-4} \text{ cm} \qquad \text{for 12 kG.}$$

Using the above 19 kG value of Δ for 18 kG, for $v_d = 6.6 \times 10^7$ cm/sec the "extra energy" available to electrons at the ends of the gap was:

$$E \cdot \Delta \approx (12 \times 10^3 \text{ V/cm}) \times (5 \times 10^{-3} \text{ cm}) \approx 60 \text{ V} \qquad \text{for 18 kG}$$
$$E \cdot \Delta \approx (8 \times 10^3 \text{ V/cm}) \times (3 \times 10^{-4} \text{ cm}) \approx 2.5 \text{ V} \qquad \text{for 12 kG.}$$

The 60 V at 18 kG could provide enough energy for several ionizing collisions, and it was large enough compared to the average electron energy of 20 eV to cause focusing of the avalanche. The 2.5 V at 12 kG, however, was too small to focus the avalance or contribute to

the ionization.

It is therefore concluded that the $E_{||}$ due to the bowing of the magnetic field lines had negligible effect on the formative time at 12 kG, but it did have an effect at 18 kG. Since the effect of $E_{||}$ can be approximated by an increase in N_0 and since the formative time depends only logarithmically on N_0, the effect contributed to the observed decrease in T_B at high values of the magnetic field but cannot be the complete explanation. For example, if the 60 V potential at 18 kG results in an increase of N_0 by a factor of ten the predicted decrease in T_B is only 10%. Also, this effect is negligible at 12 kG whereas some decrease in T_B is already observed at this value of the magnetic field. Furthermore, this effect does not predict the observed dependence of T_B on the gap spacing at the higher magnetic fields.

An additional deviation of the actual fields from those assumed in Section II was present because the electric field actually had a slight radial dependence rather than being spatially constant. It was larger near the cathode than near the anode. In a uniform electric field and with E/B and p held constant, v_E is inversely proportional to B [see Eq. (II-19)] but the ionization rate is independent of B [Eq. (II-16)]. Thus, in a high magnetic field case an avalanche starting from the cathode remains closer to the cathode as it grows than in a lower magnetic field case with the same value of E/B. With the slight radial dependence of the electric field, then, in the high magnetic field case the avalanche, because of its proximity to the cathode, grows in a slightly larger E/B than in the lower magnetic field case (even though V_g/B was held constant). Thus the ionization rate β, which is sensitive to the value of E/B (see Fig. 5), is higher for the larger magnetic field case.

Qualitatively, then, the radial dependence of the electric field is expected to cause a decrease in T_B as B is increased at constant V_g/B, d and p, in agreement with the experimental results. Furthermore, the effect is larger for the larger gap spacings, which is also in agreement with the observations. A quantitative treatment of this

effect is presented in Appendix A. It is shown there that the corrections to the formative time are only of the order of the gap spacing divided by the cathode radius and are too small to explain the experimental results.

B. Impurities and Electrode Surface Effects

It has been reported by others[6,17] that (traces of) gas impurities are not an important source of errors in ionization measurements when the test gas is hydrogen, and it is believed that this was also the case in the present experiment. There was no noticeable dependence of the formative time on the base pressure of the vacuum system, on how long it had been since the system was let up to air, or on whether or not the cold-trap in the vacuum system was used. Furthermore, there was no noticeable change in the formative time when at the end of a run the vacuum system was let up to air for 10 min and then pumped down again for a couple of hours and a few points rechecked.

These observations are also consistent with the assertion that electrode surface effects were not important for the primary avalanche breakdown conditions of this experiment. On the other hand, the fact that the formative time was slightly dependent on the time interval between breakdown initiations indicates the presence of surface effects--either at the electrodes or at the end insulators.

Other than by the mere presence of a small percentage of matter with an ionization cross section different from that of the test gas, the usual effects that one expects from impurities are:

(1) They can be photoionized either from their ground state or from a metastable state and thus provide a "cheap" source of electrons.

(2) They can be ionized by inelastic collisions with metastables of the test gas.

(3) They can significantly alter the electron distribution function (and therefore affect the ionization of the test gas) in such a way as to cool the electrons by introducing important new energy loss mechanisms for low energy electrons.

(In addition, mercury vapor has a long history[10] of causing errors in α measurements in hydrogen when mercury diffusion pumps are used, but such was not the case here.) At the low pressures of the present experiment the mean free path for photoionization for a typical process is about 75 cm or larger for an impurity level of about 1%. Thus photoionization processes are not important here. Furthermore, metastable effects in hydrogen are not expected to be important, especially in a pulsed experiment. Finally, although important in noble gases the third effect above is not usually important in diatomic gases. The vibrational excitation of the hydrogen molecule provides an energy sink for low energy electrons to which a low level of impurities can add only a small effect.

As was stated in the introduction, secondary electron production is not believed to be an important process in this experiment. Nevertheless, as the primary avalanche grows and moves across the gap there will indeed be secondary electrons produced at the cathode by ion and photon bombardment. A rough estimate of the importance of these secondary electrons can be obtained by considering a one-dimensional model of the electron density as a function of position and time in a linear electrode gap. The solution of this problem is outlined in Appendix C; only the model and the results are presented here.

Consider, then, a pair of infinite, plane-parallel electrodes with a gap spacing d. The magnetic field is spatially uniform and parallel to the electrode surfaces. The electric field is applied across the gap at time t = 0. It is assumed that the initial electrons are all located in a layer of n_{AO} electrons per unit area at the cathode. (This uniform distribution of the initial electrons is a poor approximation to the actual experiment, where only a small portion of the cathode was illuminated with ultraviolet light, but it is convenient for the present discussion and does not affect the nature of the result. A further discussion of the spatial distribution of the initial electrons is presented in Section VC.) The dominant secondary electron production process at the cathode is assumed to be that due to ion bombardment. The solution for the

electron density in the gap as a function of space and time for this model, neglecting diffusion, is

$$n(x,t) = n_{AO} \exp(\alpha x)\left\{\delta(v_E t - x) + \alpha\gamma \exp\left[\alpha(\gamma+1)\left(1+\frac{v_E}{V_E}\right)^{-1}(v_E t - x)\right]\right\} \qquad \text{(V-1)}$$

where $x = 0$ at the cathode and α is the first Townsend ionization coefficient and γ is the effective secondary emission coefficient. This expression can be integrated with respect to x to obtain the number of electrons per unit area in the gap, n(t). (This quantity corresponds to N(t) in the three dimensional case.) Doing so yields

$$n(t) = n_{AO} \exp(\beta t)\left\{1 + \gamma \frac{1 - \exp\left[-\beta t\left(\frac{v_E}{V_E} - \gamma\right)\left(1+\frac{v_E}{V_E}\right)^{-1}\right]}{1 - (\gamma+1)\left(1+\frac{v_E}{V_E}\right)^{-1}}\right\} \quad \gamma \neq \frac{v_E}{V_E} \qquad \text{(V-2)}$$

$$n(t) = n_{AO} \exp(\beta t)\left[1 + \gamma\beta t\right] \quad \gamma = \frac{v_E}{V_E} \qquad \text{(V-3)}$$

In each of these expressions the first term represents the primary avalanche and the term proportional to γ represents the contribution from the secondary electrons.

It is demonstrated in Appendix B that for the conditions of this experiment the relation $v_E/V_E \ll 1$ was usually valid. In fact a typical value for this ratio was 10^{-1}.

The secondary coefficient γ_i for electron production by ion bombardment in the absence of a magnetic field depends on the material and the nature of the surface and also on the energy of the incoming ion. When there is a strong magnetic field parallel to the cathode surface the effective secondary coefficient γ differs from γ_i because many of the electrons are returned to the cathode by the magnetic field. In order to escape recapture by the surface a secondary electron must make a collision before it returns to the cathode. Since the probability for this is of order $(\omega_b \pi)^{-1}$, a reasonable estimate for γ is

$$\gamma \approx \gamma_i (\omega_b \tau)^{-1}.$$

It is shown in Appendix B that a typical ion velocity is 10^7 cm/sec, which implies an ion energy of 100 eV. Any estimate for γ_i would have to be a guess, especially for a complicated surface like the oxide covered, gas laden aluminum cathode of this experiment. A reasonable guess for γ_i is perhaps 10^{-2}.[18,19] Then, since $10 < \omega_b \tau < 350$, γ was probably around 10^{-3} or 10^{-4}. At any rate, a reasonable match of Eq. (V-2) to the experiment can be obtained by taking the limit $1 \gg v_E/V_E \gg \gamma$. Doing so yields

$$n(t) \approx n_{A0} \exp(\beta t) \left\{ 1 + \gamma \frac{V_E}{v_E} \left[1 - \exp\left(- \frac{v_E}{V_E} \beta t \right) \right] \right\}. \qquad \text{(V-4)}$$

It is thus seen that the correction term is small and therefore the secondary electrons are indeed not important.

In this estimate of the magnitude of the effect of the secondary electrons for convenience it has been assumed that the dominant production mechanism at the cathode is due to ion bombardment. Actually, it is expected that the photoelectron production will be comparable to the production by 100 eV ions but not so large as to alter the conclusion that secondary electrons are not important.

C. Initial Electron Effects

Another possibility of explaining the observed decrease in $n_g T_B$ as E and B are increased, keeping E/B constant, lies in allowing for a changing N_0. That is, the assumption

$$\beta T_B = \ln \frac{N(T_B)}{N_0} = \text{constant}$$

of Section IIE is replaced by

$$N(T_B) = \text{constant}.$$

Then T_B changes with N_0 according to the relation

$$\beta T_B = \ln \frac{N(T_B)}{N_0} = \text{constant} - \ln N_0.$$

It does not seem likely, however, that the observed decrease in $n_g T_B$ is due to an increase in N_0 (by some unspecified process) because T_B depends only logarithmically on N_0. Thus to explain the 0.8 cm gap data of Fig. 16, for example, an increase of about 10^5 in N_0 is required as E and B are increased by a factor of 3 from their values at B = 6 kG. In addition, as a result of increasing B and therefore $\omega_b\tau$ one would actually expect a decrease in N_0 because the resulting increase in $\omega_b\tau$ implies a higher probability that the secondary electrons from the ultraviolet radiation will be recaptured by the cathode.

Heretofore there has been no discussion of the spatial distribution of the initial electrons, except that they have been assumed to be located at the cathode. The actual spatial distribution of the initial electrons was determined by the steady-state diffusion away from the small illuminated area of the cathode, for the ultraviolet illumination was continuous during the operation of the experiment. During the time of the diffusion now under consideration there was, of course, no applied electric field and the electrons were cold.

Even using the approximation of a linear gap and even though it is steady state, this is a complex diffusion problem, for it involves anisotropic diffusion and somewhat complicated boundary conditions. However, the fact that the boundaries of the ends of the gap were insulators permits the great simplification of reducing the problem to two-dimensional diffusion (of a Lorentz gas) across a magnetic field; for these end insulators charge up enough to stop the axial electron flow, and then the electron density in the axial direction is essentially constant except in a small sheath region at the insulators. This two-dimensional isotropic diffusion problem consisting of two sinks (the anode and the cathode) and a source (the illuminated portion of the cathode) can certainly be solved, for example by conformal mapping techniques, but the detailed solution is not necessary here. Instead it will just be noted that, although the distribution

is complicated, the density falls off more or less linearly as one moves across the gap from the source and more or less exponentially as one moves along the gap (i.e. azimuthally) away from the source region.

The important point here is that with the ultraviolet illumination the initial electrons were not actually all at the cathode but were rather distributed in the gap uniformly along B and nonuniformly perpendicular to B by diffusion. Thus the model of the avalanche starting from the surface of the cathode is a bit crude, and the discussion at the end of Section VA of the effect of the radial variation of E on the formative time may not apply. On the other hand, the comparison of the formative times and the shot-to-shot reproducibility with and without the ultraviolet illumination presented in Section IIIA seems to indicate that the main effect of the ultraviolet light was to provide initiating electrons and that their distribution was unimportant.

In an attempt to assess the importance of the spatial distribution of the initial electrons, the one-dimensional problem of the charged particle density in a linear gap as a function of space and time with the initial condition of a uniform distribution of n_0 electrons per unit volume throughout the gap can be solved in a manner analogous to that outlined in Appendix C. (This case represents an opposite extreme from the δ function initial condition used in Appendix C.) The results are:

Region I $\quad d \geq x > v_E t$

$$n(x,t) = n_0 \exp(\beta t)$$

$$n^i(x,t) = n_0 \exp(\beta t)\left[1 - \exp\left(-\beta \frac{d-x}{V_E}\right)\right] \qquad t > \frac{d-x}{V_E}$$

Region II $\quad v_E t > x \geq 0 \qquad t > \frac{d}{V_E}$

$$n(x,t) = n_0\left(\frac{V_E}{v_E}\gamma A \exp B - C\right)$$

$$n^i(x,t) = n_0\left\{A \exp D - \exp\left[\beta\left(t - \frac{d-x}{V_E}\right)\right] - C\right\}$$

where
$$A = 1 + \gamma\left(\frac{v_E}{V_E} - \gamma\right)^{-1} \exp\left(-\frac{\beta d}{V_E}\right)$$

$$B = \alpha x + \alpha(1 + \gamma)\left(1 + \frac{v_E}{V_E}\right)^{-1}(v_E t - x)$$

$$C = \gamma\left(\frac{v_E}{V_E} - \gamma\right)^{-1} \exp\left[\beta\left(t - \frac{d}{V_E}\right)\right]$$

$$D = \beta(1 + \gamma)\left(1 + \frac{v_E}{V_E}\right)^{-1}\left(t + \frac{x}{V_E}\right) - \beta\gamma\,\frac{x}{v_E}\,.$$

The author has used these expressions to determine the electric field at the anode as a function of time in an attempt to obtain a different criterion for breakdown. The resulting expression was rather complicated (even in the limit $1 \gg v_E/V_E \gg \gamma$) and did not seem to lead to any new results.

The electron and ion densities given by these results are shown qualitatively for $t = (1/2)(d/v_E)$ in Fig. 21. As time progresses the densities increase in magnitude as $\exp(\beta t)$ and the discontinuity in the electron density moves toward the anode with velocity v_E. This discontinuity marks the position of the electrons that were initially at the cathode. The electrons between the discontinuity and the cathode at any time are the result of secondary production at the cathode.

D. Electron Losses

The principal loss of electrons from the avalanche is along the magnetic field to the end insulators. For a first estimate, the loss of electrons due to ordinary diffusion is considered in order to establish that the end loss may indeed be significant. The electrons are assumed to be chargeless particles in that the space charge effects and the effects due to curvature of the magnetic field lines are ignored. The end insulators are considered to be sinks.

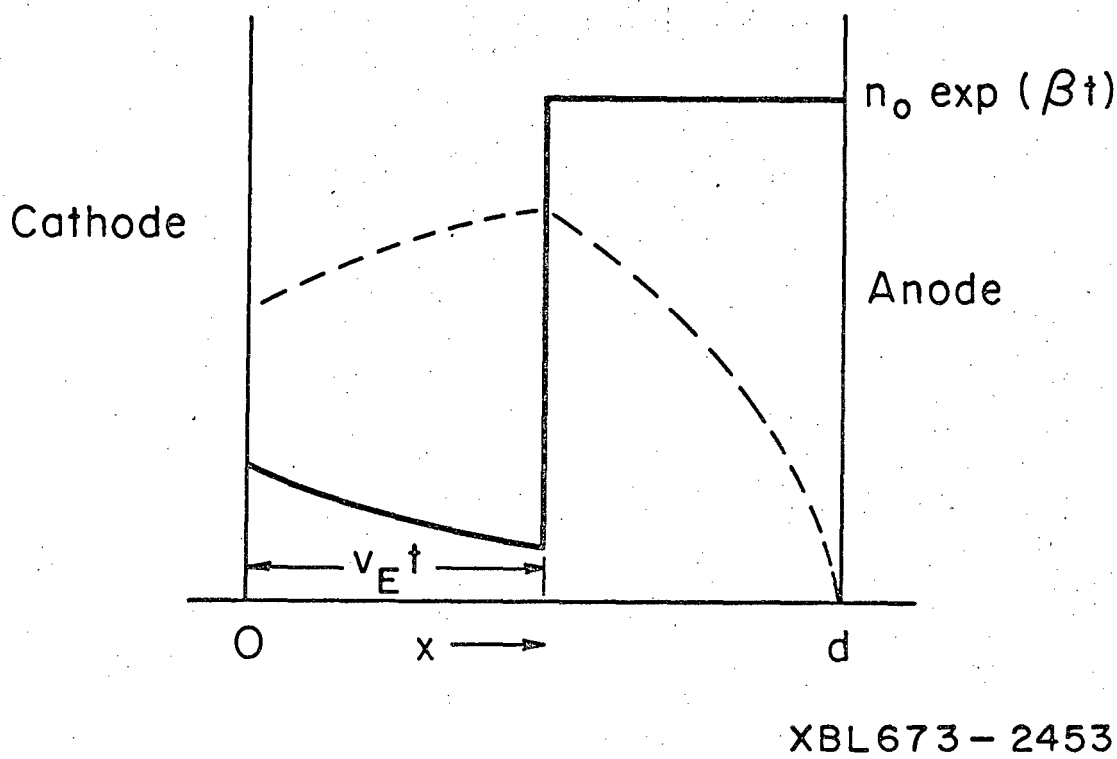

Fig. 21. A qualitative diagram of the charged particle densities at $t = (1/2)(d/v_E)$ for a uniform distribution of the initial electrons. The solid line is the electron density and the dotted line is the ion density.

Under these conditions the average time T_D between the production of an electron and its loss to the ends by diffusion is given approximately by

$$T_D \approx \frac{h^2}{\pi^2 D_{\|}} \qquad \text{(V-5)}$$

where h = 8.5 cm is the height (i.e. length in axial direction) of the electrodes. Using this value for h and also the relations

$$D_{\|} \approx \frac{1}{3} \frac{\langle v^2 \rangle}{\nu_c} \quad \text{cm}^2/\text{sec}$$

$$\nu_c \approx 4 \times 10^9 p \quad \text{sec}^{-1}$$

$$\langle v^2 \rangle \approx 36 \times 10^{14} \overline{\epsilon}(\text{eV}) \quad \text{cm}^2/\text{sec}^2$$

$$\overline{\epsilon} \approx 3 \frac{E}{B} \times 10^{-2} \quad \text{eV},$$

where the expression for $D_{\|}$ is an approximation for Eq. (II-11) and the expression for $\overline{\epsilon}$ is an approximation suggested by the numerical calculation of Pearson and Kunkel,[9] one obtains from Eq. (V-5):

$$T_D \approx p \left(\frac{B}{E} \right) \times 10^3 \quad \mu\text{sec}. \qquad \text{(V-6)}$$

(The units for p, B, and E here are those listed at the end of Section I.)

A sufficient condition for this diffusion loss to be negligible is the requirement that $T_D \gg T_B$. A less restrictive but very necessary condition is that $T_D > \beta^{-1}$. Serious difficulties are expected if this latter requirement is not met because then an electron is likely to be lost before it can make an ionizing collision. The relation $T_D > \beta^{-1}$ can be expressed in the form of a requirement on the gas pressure by means of Eq. (V-6) and Eq. (II-28). The result for the most restrictive case (i.e. $v_d = 3.3 \times 10^7$ cm/sec) is

$$p > 0.11 \text{ torr}.$$

(It was this requirement that was used to set the lower limit of the experimental pressure range at 0.2 torr.)

Using Eq. (V-6) and Eq. (II-36), the relation $T_D > T_B$ can also be expressed in terms of the gas pressure. The result is:

$$p > 0.55 \text{ torr} \qquad v_d = 3.3 \times 10^7 \text{ cm/sec}$$
$$p > 0.37 \text{ torr} \qquad v_d = 5.0 \times 10^7 \text{ cm/sec}$$
$$p > 0.32 \text{ torr} \qquad v_d = 6.6 \times 10^7 \text{ cm/sec.}$$

At the lowest pressures of this experiment these conditions were in general not met.

The conditions obtained here are admittedly only very approximate since they fail to take into account complications arising from the fact that an electron is a charged particle. Nevertheless, on the basis of them it seems very likely that the greater shot-to-shot scatter at the lower pressures and also the deviation in linearity with $1/p$ observed in Fig. 14 can be attributed to electron losses to the end insulators.

The condition $T_D \gg T_B$ was not met at all in the experiment. This means that the electron losses to the end insulators should be taken into account in explaining the experimental observations. A simple way to do this is to replace the equation (of continuity)

$$\frac{dN}{dt} = \beta N$$

which underlies Eq. (II-1) by the more complete expression

$$\frac{dN}{dt} = \beta N - \left(\frac{dN}{dt}\right)_{loss} = \beta' N \qquad \text{(V-7)}$$

where
$$\beta' = \beta - \frac{1}{N}\left(\frac{dN}{dt}\right)_{loss} . \qquad \text{(V-8)}$$

For the diffusion loss one then has

$$\beta' = \beta - \frac{1}{T_D} .$$

Next it is necessary to consider the end losses in more detail,

taking into account the effects of electric fields. Three processes which lead to these end losses are:

(1) Just before the gap voltage is pulsed on at the beginning of the breakdown the initial electrons are cold and the end insulators have sufficient charge to lower the potential at their surface about 1/25 eV in order to halt the axial electron flow. Upon establishing the electric field across the gap, however, the mean electron energy quickly rises to about 15 eV (for $v_d = 5.0 \times 10^7$ cm/sec), and the axial electron flow resumes until the end insulators have accumulated enough charge to lower their surface potential to about 15 V below its vacuum value.

(2) In addition, the avalanche moves azimuthally around the gap so that it continually comes into contact with fresh insulator surface which also needs to be charged.

(3) Towards the end of the formative time the space charge potential of the electron avalanche becomes comparable to and then larger than the mean electron (thermal) energy. When this occurs additional charge flows to the end insulators in order to establish an $E_{||}$ sufficiently large to overcome the space charge repulsion in the avalanche.

The capacity per unit area C_A between the inside surface of the end insulator and the end resistor (which was held at the vacuum potential) on its outer surface was about 2 pF/cm^2 for each end insulator. The number of electrons per unit area required to charge this capacitance to 15 V was about 4×10^8/cm^2. Thus the end insulators acted as sinks and the electron loss to them was significant for more than half of the formative time.

The complete, time-dependent diffusion problem for the electron end losses is difficult, for the electron axial flow is controlled by the density gradient and the self-consistant space charge potential along with the time varying boundary conditions. This problem has not been solved. Interestingly, this complex loss process along the magnetic field to the ends apparently deviates only weakly from a linear pressure dependence, for the observed pressure dependence of T_B

indicates that β' was proportional to the pressure.

It is not expected that the magnetic field intensity alone would have much effect on the end losses as long as E/B is held constant so that the mean electron energy remains fixed. However, the $E_{\|}$ component of the electric field due to the bowing of the magnetic field lines is expected to exert a restraining influence on the end losses. The decrease in T_B with increasing B (at constant E/B) exhibited in Figs. 16 through 19 is tentatively attributed to this effect.

E. The Assumption of Constant βT_B

Finally, it might be questioned whether the decrease in T_B with increasing B illustrated in Figs. 16 through 19 could be attributed to a failure of the assumption that βT_B equals a constant independent of the pressure of the applied fields. This seems rather unlikely, because to attribute the factor-of-two decrease in the observed T_B to a decrease in βT_B would imply a tremendous decrease in the multiplication factor (or alternatively the charged particle density) at breakdown--namely from about 10^{11} to about 10^{6}. It seems much more likely that the change in the observed breakdown time must be attributed to a change in β, with βT_B being approximately constant. In this case the experiment did not test the assumption that βT_B equals a constant because any change in the value of this product was hidden by the large change in β.

VI. CONCLUSION

Reproducible values for the formative time of breakdown across a strong magnetic field have been measured for conditions where this time is less than the time required for an electron to drift across the electrode gap (in the vacuum fields). These measurements are compared with a simplified theory which neglects electron losses from the avalanche. The pressure dependence of the formative time predicted by this theory was confirmed over a range of pressures spanning a decade. The functional dependence of the formative time on E/B predicted by the theory was not observed; at constant E/B the formative time, rather than being constant, decreased about a factor of two as the magnetic field increased by a factor of three. The magnitudes of the formative time were in reasonable agreement with the theory (and supported the experimental measurements of the First Townsend ionization coefficient) if it is assumed that the high magnetic field values are best because the deviations from them were due to electron losses along the magnetic field.

In general, the pressure dependence agreement and the agreement with predicted magnitudes seem to indicate that the theoretical discussion of the breakdown here is at least partially correct. It is argued further that one expects electron losses along the magnetic field to be serious and that a more complete theory which takes them into account is necessary.

The observed magnitudes of the formative time suggest curve 5 of Fig. 5 to be the best of the curves presented there as an estimate for the ionization frequency in the range of this experiment. In principal a better determination of the ionization frequency could, of course, be made by the much more difficult but direct method of measuring the electrical current through the gap as a function of time, but the electron losses along the magnetic field would still have to be either eliminated or adequately taken into account.

ACKNOWLEDGMENTS

The author wishes to express his thanks to Dr. Wulf B. Kunkel for much encouragement and many invaluable discussions during the course of this work. The interest and aid of William R. Baker were also very helpful. In addition, the support of Dr. C. M. Van Atta is gratefully acknowledged.

This work was performed under the auspices of the U. S. Atomic Energy Commission.

APPENDICES

A. The Effect of the Radial Dependence of the Electric Field on the Formative Time

If the ionization frequency for the electrons in an avalanche changes (in this case because of the motion of the avalanche in the nonuniform electric field), the number of electrons in the avalanche as a function of time is given by

$$N(t) = N_0 \exp\left[\int_0^t \beta(t')dt'\right]$$

where any losses of electrons are neglected. For an avalanche starting from the cathode this relation can be equivalently expressed in terms of x, the distance of the avalanche from the cathode, by

$$N(x) = N_0 \exp\left[\int_0^x \alpha(x')dx'\right]. \qquad \text{(A-1)}$$

This second form will be used here. Figure 22 explains the notation employed.

It is desired to compare the formative times in the curved gap of this experiment for two cases, which are here labeled (1) and (2), having the same gas pressure p, the same gap length d, and the same ratio V_g/B but having different magnetic fields. Thus

$$\frac{V_g^{(1)}}{B^{(1)}} = \frac{V_g^{(2)}}{B^{(2)}}, \qquad \omega_b{}^{(1)}\tau \neq \omega_b{}^{(2)}\tau. \qquad \text{(A-2)}$$

To facilitate this comparison, first the formative time in the curved gap is compared with that in a plane gap for the same p, B, d, and V_g. A correction to the formative time due to the slightly nonuniform electric field is thus obtained. The two curved cases (1) and (2) are then compared by comparing each to its corresponding plane gap case and using the theory presented in Section II to relate these two plane gap cases.

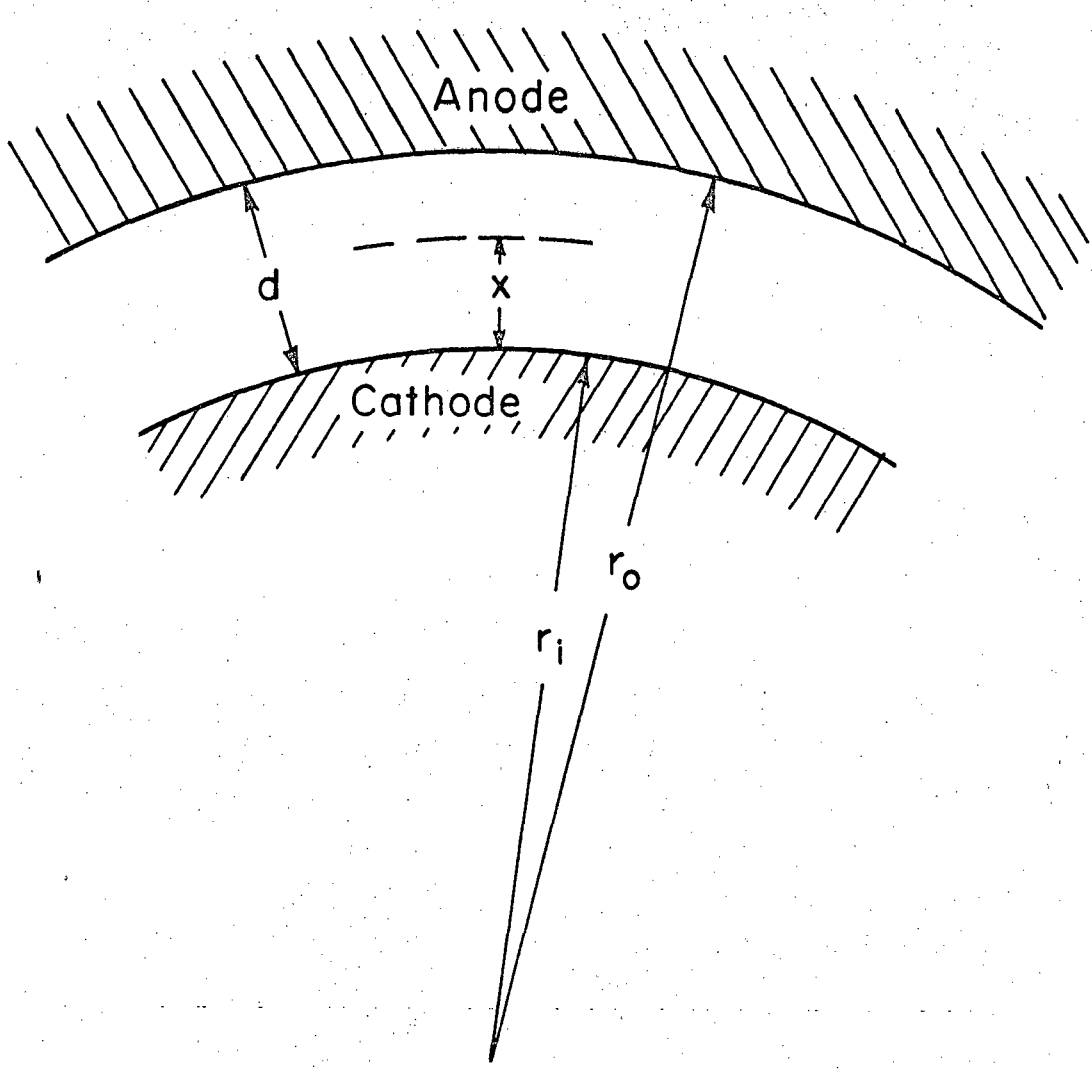

XBL673-2454

Fig. 22. Explanation of the symbols used in the discussion of the effect of the radial dependence of the electric field. x is a position variable designating the distance from the cathode.

To begin, then, the curved gap case (r) is compared with a plane gap case (s) with the same p, B, d, and V_g. The electric fields in the two cases are

$$E^{(s)} = \frac{V_g}{d}$$

$$E^{(r)}(x) = \frac{V_g}{(r_i + x) \ln (r_o/r_i)} . \qquad (A-3)$$

In keeping with the assumption that the formative time is inversely proportional to the ionization rate, the formative times are compared on the basis that N/N_0 be the same in the two cases. From Eq. (A-1) this assumption requires

$$\int_0^{x^{(r)}} \alpha^{(r)}(x')dx' = \int_0^{x^{(s)}} \alpha^{(s)}(x')dx' \qquad (A-4)$$

where $x^{(r)} \equiv x(T_B^{(r)})$ is the position in the gap at time $T_B^{(r)}$ of an avalanche that started at the cathode at time zero.

The expression for α given by Eq. (II-26) is adequate for this analysis because the range of E/B is very small here. Using this expression Eq. (A-4) becomes

$$\int_0^{x^{(r)}} \left[\exp\left(-C_2 \frac{B}{E^{(r)}(x')}\right)\right]dx' = \int_0^{x^{(s)}} \left[\exp\left(-C_2 \frac{B}{E^{(s)}}\right)\right]dx' . \qquad (A-5)$$

Using Eq. (A-3) in Eq. (A-5), upon integrating one obtains

$$\frac{V_g}{C_2 B \ln (r_o/r_i)}\left[1 - \exp\left(-C_2 \frac{B}{E(0)} \frac{x^{(r)}}{r_i}\right)\right] = x^{(s)} \exp\left[- C_2 \frac{Bd}{V_g}\left(1 - \frac{r_i}{d} \ln \frac{r_o}{r_i}\right)\right] \qquad (A-6)$$

where $E(0) = V_g\left[r_i \ln (r_o/r_i)\right]^{-1}$ is the electric field at the cathode in the curved gap geometry. Since C_2 is of the same order of magnitude as E/B, the argument of the exponential term on the left hand side of

Eq. (A-6) is of order d/r_i. The magnitude of d/r_i ranges from about 1/7 for a 1 cm gap spacing down to about 1/25. Upon expanding this exponential term, Eq. (A-6) becomes

$$x^{(r)}\left[1 - \frac{C_2 B \ln (r_o/r_i)}{2V_g} x^{(r)}\right] \approx x^{(s)} \exp\left[-C_2 \frac{Bd}{V_g}\left(1 - \frac{r_i}{d} \ln \frac{r_o}{r_i}\right)\right]. \quad \text{(A-7)}$$

Let $x' \equiv x(t')$ be the radial position in the curved gap at time t' of an avalanche that was born at the cathode at time zero. Then

$$dx' = v_E(x')dt'. \quad \text{(A-8)}$$

For notational convenience and for ease in evaluating the magnitude of correction terms, the approximate Eq. (II-18) for v_E is used here. This is not necessary; one could just as well use the symbolic form $v_E = \mu_E E$ or alternatively the more cumbersome form of Eq. (II-19). From Eq. (II-18), then

$$v_E(x') = \frac{10^5 E(x')}{\omega_b \tau B} \text{ cm/sec} \quad \text{(A-9)}$$

where E is in volts/cm and B is in kG. Using Eqs. (A-3) and (A-9), Eq. (A-8) can be integrated. The result is

$$x' = r_i\left[\left(1 + \frac{2 \times 10^5}{\omega_b \tau} \frac{E(0)}{r_i B} t'\right)^{1/2} - 1\right]. \quad \text{(A-10)}$$

The term containing t' is of order $v_E t'/r_i$, which in turn is of order d/r_i for the times of interest. Therefore the square root term can be expanded.

$$x' \approx \frac{10^5 E(0)}{\omega_b \tau B} t' \left(1 - \frac{1}{2} \frac{10^5}{\omega_b \tau} \frac{E(0)}{r_i B} t'\right) \text{ cm.} \quad \text{(A-11)}$$

Using Eq. (A-11) and its obvious companion for the straight gap, $x^{(s)} = v_E t^{(s)}$, in Eq. (A-7) and dropping terms of higher than first order in d/r_i, one obtains the desired relationship between the formative times:

$$T_B^{(r)}\left[1 - \frac{10^5}{2r_i}\frac{E(0)}{\omega_b \tau B}\left(1 + C_2 \frac{B}{E(0)}\right)T_B^{(r)}\right] \approx$$

$$T_B^{(s)}\left(\frac{r_i}{d}\ln\frac{r_o}{r_i}\right)\exp\left[-C_2\frac{Bd}{V_g}\left(1 - \frac{r_i}{d}\ln\frac{r_o}{r_i}\right)\right]. \qquad \text{(A-12)}$$

In the limit $r_i \to \infty$, Eq. (A-12) becomes $T_B^{(r)} = T_B^{(s)}$ as it should. The correction term on the right hand side arises because of the comparison of a curved gap with a straight gap. It is of a geometrical nature and cancels out in the comparison of the two curved gap cases (1) and (2). The factor on the left hand side of the equation contains the effect of the avalanche motion away from the cathode in the nonuniform electric field.

Since terms of higher than first order in d/r_i have already been dropped from the left hand side of Eq. (A-12), the geometrical factor on the other side can be expanded to this same order. Doing so, Eq. (A-12) takes the following form:

$$T_B^{(r)}\left[1 - \frac{x_B(0)}{2r_i}\left(1 + C_2\frac{B}{E(0)}\right)\right] \approx T_B^{(s)}\left[1 - \frac{d}{2r_i}\left(1 + C_2\frac{B}{E^{(s)}}\right)\right]. \qquad \text{(A-13)}$$

Here $x_B(0) \equiv \left[10^5 E(0)/\omega_b \tau B\right] T_B^{(r)}$ is the position the avalanche would have had at actual breakdown if the electric field had remained constant at $E(0)$. [The actual position at breakdown $x^{(r)}(T_B^{(r)})$ is of course slightly less than $x_B(0)$ because of the decrease of the electric field away from the cathode.] Equation (A-13) makes it evident that

$$T_B^{(r)} = T_B^{(s)}\left[1 + O\left(\frac{d}{r_i}\right)\right]$$

where O denotes "order of magnitude", as was already apparent because the correction terms are of order d/r_i. Therefore, within the accuracy of the expansions employed, the $T_B^{(r)}$ in the correction term in

Eq. (A-12) can be replaced by $T_B^{(s)}$; also, E(0) can be replaced by $E^{(s)}$. Thus Eq. (A-12) can be written

$$T_B^{(r)}\left[1 - \frac{10^5 V_g}{2r_i\omega_b\tau Bd}(1 + C_2)\frac{Bd}{V_g}T_B^{(s)}\right] \approx T_B^{(s)}\left[1 - \frac{d}{2r_i}\left(1 + C_2\frac{Bd}{V_g}\right)\right] . \quad \text{(A-14)}$$

Equation (A-14) is now used to compare the curved gap cases (1) and (2). Since V_g/B is the same for these two cases, C_2 is also the same. Furthermore, $T_B^{(s)}(1) = T_B^{(s)}(2)$ according to the results of Section II [see Eq. (II-30)]. Therefore

$$T_B^{(r)}\left[1 - \frac{10^5 V_g}{2r_i\omega_b^{(1)}\tau Bd}\left(1 + C_2\frac{Bd}{V_g}\right)T_B^{(s)}\right] \approx$$

$$T_B^{(r)}(2)\left[1 - \frac{10^5 V_g}{2r_i\omega_b^{(2)}\tau Bd}\left(1 + C_2\frac{Bd}{V_g}\right)T_B^{(s)}\right]$$

which can also be written

$$\frac{T_B^{(r)}(1)}{T_B^{(r)}(2)} \approx 1 - \frac{10^5 V_g}{2r_i Bd}\left(1 + C_2\frac{Bd}{V_g}\right)T_B^{(s)}\left(\frac{1}{\omega_b^{(2)}\tau} - \frac{1}{\omega_b^{(1)}\tau}\right) . \quad \text{(A-15)}$$

From Eq. (A-15) it can be seen that if $B^{(1)}$ is larger than $B^{(2)}$, $T_B^{(r)}(1) < T_B^{(r)}(2)$ at constant E/B. This is in qualitative agreement with the experimental observations. Indeed, it was the anticipation of this result that led to the present analysis in the first place. Unfortunately, however, the magnitude of the effect is not large enough to explain the data. For example, consider Fig. 16, which shows the data for the 8 mm gap. For the $v_d = 6.6 \times 10^7$ cm/sec case, using

$$\frac{V_g}{Bd} = 660 \frac{\text{volts/cm}}{\text{kG}}$$

$$C_2 = 700 \frac{\text{kG cm}}{\text{volts}}$$

$$\omega_b\tau = 3.5\ B/p$$

$$r_i = 7.45 \text{ cm}$$

$$n_g T_B^{(s)} = 8 \times 10^9 \text{ sec/cm}^3$$

Eq. (A-15) yields

$$\frac{T_B^{(r)}\ (18 \text{ kG})}{T_B^{(r)}\ (6 \text{ kG})} = (1 - 0.07).$$

Similarly for the $v_d = 5 \times 10^7$ cm/sec case, Eq. (A-15) yields an 11% correction between $T_B^{(r)}(18 \text{ kG})$ and $T_B^{(r)}(6 \text{kG})$, and for $v_d = 3.3 \times 10^7$ cm/sec it yields a 3% correction between $T_B^{(r)}(18 \text{ kG})$ and $T_B^{(r)}(15 \text{ kG})$.

Equation (A-14) can also be used to obtain a correction to the formative time due to a change of gap length. In the experiment the gap length d was changed by the substitution of another cathode with a different diameter. To obtain the effect of changing the gap, therefore, two cases labeled (a) and (b), having the same B, p, and V_g/Bd but having different r_i and d are compared. Again Section II predicts $T_B^{(s)}(a) = T_B^{(s)}(b)$, and in the same manner that Eq. (A-15) was obtained one finds from Eq. (A-14)

$$\frac{T_B^{(r)}(a)}{T_B^{(r)}(b)} \approx 1 - \frac{1}{2}\left(\frac{d(a)}{r_i(a)} - \frac{d(b)}{r_i(b)}\right)\left(1 + C_2 \frac{B}{E}\right) + \frac{10^5 E}{2\omega_b \tau B} T_B^{(s)}\left(1 + C_2 \frac{B}{E}\right)\left(\frac{1}{r_i(a)} - \frac{1}{r_i(b)}\right). \qquad \text{(A-16)}$$

It is seen that the two correction factors are of opposite sign. The term

$$\frac{10^5 E}{2\omega_b \tau B} T_B^{(s)}\left(1 + C_2 \frac{B}{E}\right)\left(\frac{1}{r_i(a)} - \frac{1}{r_i(b)}\right)$$

can be ignored because being of $O(d^2/r_i^2)$ it is about an order of magnitude less than the other correction term. This being the case, it is seen that Eq. (A-16) predicts smaller formative times for larger gap lengths, but it does not explain the dependence of the gap length effect on the magnetic field (see Fig. 19).

As before, the magnitude of the effect predicted by Eq. (A-16) is too small to explain the observations. For a numerical example consider the following case which can be compared with Fig. 18.

$$\frac{Bd}{V_g} = \frac{1}{500}\ \frac{\text{kG-cm}}{\text{volt}} \quad (v_d = 5 \times 10^7 \text{ cm/sec})$$

$$\omega_b\tau = 3.5\,\frac{B}{p}$$

$$B = 18 \text{ kG}$$

(a) : 8 mm gap $\quad d = 0.8$ cm $\quad r_i = 7.45$ cm

(b) : 3 mm gap $\quad d = 0.3$ cm $\quad r_i = 7.95$ cm

Using $C_2 = 700$ volts/kG-cm and $n_g T_B^{(s)} = 16 \times 10^9$ sec/cm^3, Eq. (A-16) yields

$$\frac{T_B^{(r)}(8 \text{ mm})}{T_B^{(r)}(3 \text{ mm})} \approx (1 - 0.08 + 0.004).$$

So for this case Eq. (A-16) predicts an 8% decrease, whereas the observed decrease is about 25%. Furthermore, the predicted 8% difference at 18 kG would only be decreased to 7% at 6 kG; that is, the observed B dependence of the gap length effect is not predicted.

In conclusion, it has been demonstrated that the effects of the radial dependence of the electric field cannot explain the observed deviations of the formative times from strict E/B dependence, although qualitatively the effects are in the "right direction".

B. The Motion of the Ions

When an electron in the energy range of interest here makes an ionizing collision with a hydrogen molecule, the resulting ion is at least ten times more likely to be H_2^+ than H^+.[14] For the conditions of this experiment the ion cyclotron frequency was much less than the collision frequency for both of these ion species. Therefore the ion velocity distribution functions, drift velocities, etc. were functions of the parameter E/p. Since the range of E/p was 1.5 to 60 kV cm^{-1} $torr^{-1}$, it is expected that the dominant collisional process between the H_2^+ ions and the H_2 molecules was resonant charge exchange. (E/p was too high for such low energy processes as the production of H_3^+ to be important and was too low for molecular ionization or molecular breakup processes to be significant.) It is asserted, then, that the dominant ion species was H_2^+ and that these ions interacted with the parent gas primarily by means of charge exchange collisions.

For the ion energies of interest here the charge exchange cross section for H_2^+ with H_2 is nearly constant at about 8×10^{-16} cm^2.[15] This implies a mean free path of about 4×10^{-2} p^{-1} cm, where the pressure is in torr. For example, an H_2^+ ion formed in the center of a 0.5 cm gap at 1.0 torr would have suffered about six charge exchange collisions as it moved to the cathode.

Notice that each ion arriving at the cathode was preceded by a number of energetic neutrals which were products of the charge exchange collisions. This effect may be of interest in situations where secondary production or adsorbed gas release at the cathode is important.

There are no measurements for the ion mobility at these high values of E/p because such values generally imply breakdown conditions. However, the preceding discussion suggests a rough calculation for the ion drift velocity. The ions are born essentially at rest and then begin to accelerate in the direction of the electric field. It will be assumed that their motion consists of a series of accelerations from zero velocity through one mean free path followed by a charge exchange collision (which in effect stops the ion completely). Then

$$\frac{1}{2} M V_f^2 = eE\lambda_{ce} = 4 \times 10^{-2} \frac{eE}{p}$$

implies

$$V_E = \frac{V_f}{2} \approx 10^5 \sqrt{\frac{E}{p}} \text{ cm/sec} \qquad \text{(B-1)}$$

where V_E is the ion drift velocity. It is of interest to note that Eq. (B-1) agrees surprisingly well with the measurements of Rose[16] at his highest values of E/p (100 to 150 volts cm^{-1} $torr^{-1}$). Here, of course, the expression is intended to be used at even much higher values of E/p.

From Eq. (B-1) a typical value for V_E was 10^7 cm/sec, whereas from Eq. (II-17) a typical value for v_E was 5×10^5 cm/sec. Therefore the ion drift velocity in the direction of the electric field was typically much larger than that of the electrons. (Actually, for the very lowest values of $\omega_b\tau$ these two drift velocities were comparable, but for most conditions the relation $V_E \gg v_E$ was valid.) The fact that $V_E \gg v_E$ implies that as the electron cloud slowly drifted across the gap (while rapidly moving in the $\vec{E} \times \vec{B}$ direction) the ions "rained" out the back and were collected at the cathode. Thus, there was some loss of ions during the avalanche buildup.

The number of electrons in the gap as a function of time is

$$N(t) = N_0 \exp(\beta t). \qquad \text{(B-2)}$$

An expression for the corresponding quantity for the ions, $N^i(t)$, is now obtained. The rate of change of $N^i(t)$ is the production rate minus the loss rate, or

$$\frac{dN^i(t)}{dt} = \beta N(t) - \beta N(t'), \qquad \text{(B-3)}$$

where the loss term arises from the removal at the cathode of the ions that were produced at an earlier time t'. The condition relating t' to t is that the distance of the avalanche from the cathode at time t' (which is $v_E t'$) is equal to the ion drift velocity multiplied by its transit time to the cathode. That is

$$v_E t' = V_E(t - t')$$

or

$$t' = \frac{V_E}{v_E + V_E} t. \tag{B-4}$$

Using Eq. (B-2) and Eq. (B-4), Eq. (B-3) can be integrated, and the result is

$$N^i(t) = N_0\left[\frac{v_E}{V_E} + \exp(\beta t) - \left(1 + \frac{v_E}{V_E}\right)\exp\left(\frac{V_E}{v_E + V_E}\beta t\right)\right]. \tag{B-5}$$

The electrical current through the gas is given by

$$I(t) = \frac{e}{d}\left[N^i(t)V_E + N(t)v_E\right]$$

$$= \frac{eN_0V_E}{d}\left[\left(1 + \frac{v_E}{V_E}\right)\exp(\beta t) + \frac{v_E}{V_E} - \left(1 + \frac{v_E}{V_E}\right)\exp\left(\frac{V_E}{v_E + V_E}\beta t\right)\right] \tag{B-6}$$

where d is the gap length.

In the limit $V_E \gg v_E$ Eq. (B-5) becomes

$$N^i(t) = N_0 \exp(\beta t)\left[1 - \exp\left(-\frac{v_E}{V_E}\beta t\right)\right] \tag{B-7}$$

and Eq. (B-6) becomes

$$I(t) = \frac{eV_EN_0}{d}\exp(\beta t)\left[1 - \exp\left(-\frac{v_E}{V_E}\beta t\right)\right]. \tag{B-8}$$

Notice that for later times such that $\beta t > V_E/v_E$, Eq. (B-7) approaches $N^i(t) \approx N(t)$. This is an expression of the fact (common in population explosion situations) that, because of the exponential nature of the growth, eventually practically all of the ions that have been formed in the avalanche are present, even though there has been loss. Also,

$$n_S(x,t) = n_S\left(0,\ t - \frac{x}{v_E}\right) \exp(\alpha x) \qquad (C\text{-}4)$$

and

$$n_S(0,t) = \gamma \frac{V_E}{v_E} n^i(0,t) \qquad (C\text{-}5)$$

where γ is the effective secondary coefficient for ion bombardment in a strong magnetic field. Combining the above expressions one obtains the following equation for the electron density in terms of the ion density at the cathode at an earlier time.

$$n(x,t) = n_{OA}\delta(x - v_E t) \exp(\alpha x) + \frac{V_E}{v_E} \gamma n^i\left(0,\ t - \frac{x}{v_E}\right) \exp(\alpha x) \qquad (C\text{-}6)$$

Let $y(t)$ denote the position of the primary avalanche at time t. That is, $y(t) \equiv v_E t$. Then

$$n_P{}^i\left[y(t),t\right] = \frac{1}{V_E}\frac{d}{dt} n_P = n_{AO}\frac{\beta}{V_E} \exp(\beta t).$$

Due to the finite ion drift velocity,

$$n_P{}^i(0,t) = n_P{}^i\left[y(t''),t''\right]$$

where $$t'' = \left(1 + \frac{v_E}{V_E}\right)^{-1} t. \qquad (C\text{-}7)$$

Thus

$$n_P{}^i(0,t) = n_{AO}\frac{\beta}{V_E} \exp\left[\beta\left(1 + \frac{v_E}{V_E}\right)^{-1} t\right]. \qquad (C\text{-}8)$$

The ion density at time t at the cathode due to secondary electrons is given by the integral (from the cathode out to the maximum distance for contributions to be at the cathode at time t) of V_E^{-1} times the rate of ion production by secondary electrons per unit volume at x

and a time adjusted for the ion drift velocity. That is,

$$n_S^{\,i}(0,t) = \frac{1}{V_E}\int_0^{v_E t''} \frac{d}{dt}\, n_S\left(x,\ t - \frac{x}{V_E}\right)dx$$

$$= \frac{\beta}{V_E}\int_0^{v_E t''} n_S\left(x,\ t - \frac{x}{V_E}\right)dx \qquad \text{(C-9)}$$

where t" is given by Eq. (C-7). Using Eqs. (C-4), (C-5), (C-2), and (C-8), the following integral equation for $n_S^{\,i}(0,t)$ can be obtained from Eq. (C-9).

$$n_S^{\,i}(0,t) = \frac{\beta\gamma}{v_E}\int_0^{v_E t''} n_S^{\,i}\left[0,\ t - \frac{x}{V_E}\left(1 + \frac{v_E}{V_E}\right)\right]\exp(\alpha x)dx$$

$$+ n_{AO}\frac{\beta^2\gamma}{V_E}t''\exp(\beta t'') \qquad \text{(C-10)}$$

The solution to Eq. (C-10) is

$$n_S^{\,i}(0,t) = n_{AO}\frac{\beta}{V_E}\left\{\exp\left[\gamma\beta\left(1 + \frac{v_E}{V_E}\right)^{-1}t\right] - 1\right\}\exp\left[\beta\left(1 + \frac{v_E}{V_E}\right)^{-1}t\right]. \qquad \text{(C-11)}$$

Combining Eqs. (C-2), (C-8), and (C-11) with Eq. (C-6), the solution for the electron density is finally obtained.

$$n(x,t) = n_{AO}\exp(\alpha x)\left\{\delta(v_E t - x)\right.$$

$$\left. + \alpha\gamma\exp\left[\alpha(\gamma+1)\left(1 + \frac{v_E}{V_E}\right)^{-1}(v_E t - x)\right]\right\} \qquad \text{(C-12)}$$

D. List of Symbols

B	Magnetic field intensity.
c	Velocity of light.
C_1, C_2	Constants in Eq. (II-26) for β.
C_A	Capacity/area between the inside of an end insulator and its end resistor.
C_e	Capacity between the ends of the electrodegap and the surrounding grounds.
C_0	Capacity of the main (driving) capacitor.
d	Dimension of the electrode gap in the direction of $\vec{E}$.
$D_{\parallel}$	Diffusion coefficient in the direction of $\vec{B}$.
D_E	Diffusion coefficient transverse to $\vec{B}$.
$D_{\perp}$	The off-diagonal element of the diffusion tensor.
e	Charge of an electron.
E	Electric field.
$E(0)$	Electric field at the cathode.
$E_{\parallel}$	Component of the electric field in the direction of $\vec{B}$.
f	Electron distribution function.
$f_0(v)$	Velocity-space portion of the separable electron distribution function.
$\vec{F}$	Force exerted on the electron cloud by the gas wind.
F, F_1, G	Unspecified functions used to demonstrate functional dependences.
h	Height of the electrodes.
$I(t)$	Electrical current.
I_0	Initial electric current.
K	A constant.
m	Mass of an electron
M	Mass of a hydrogen molecule.
n	Number density of the electrons.
$n^i(x,t)$	Ion number density.
n_{A0}	Initial number of electrons per unit area at the cathode.

n_g	Number density of the gas molecules.
n_o	Initial electron density.
$N(t)$	Total number of electrons in an avalanche.
$N^i(t)$	Total number of ions in an avalanche.
N_o	Initial number of electrons in an avalanche.
p	Gas pressure.
p_o	Gas pressure in torr at 20^oC.
q	Electric charge of a particle.
r_i	Inside radius of the gap.
r_o	Outside radius of the gap.
R	Series resistance in the discharge circuit.
t	Time.
t'	Time (dummy variable).
t''	$1 + \frac{v_E}{V_E} - 1$ t, an adjusted time taking into acount the finite ion drift velocity
T_B	Formative time.
T_c	Time required for an electron to cross the gap.
T_D	The lifetime of an electron before it is lost to the ends of the gap.
v	Electron velocity variable.
$\vec{v}'$	Electron velocity in the drift frame.
v_d	$10^5 E/B$; drift velocity in $\vec{E} \times \vec{B}$ direction.
$\vec{v}_d$	$c(\vec{E} \times \vec{B})/B^2$
v_E	Drift velocity of electrons along $-\vec{E}$.
V_E	Drift velocity of ions along $\vec{E}$.
V_g	Gap voltage.
V_o	Voltage initially applied across the gap; voltage to which main capacitor is charged.
x	Position variable measuring the distance in the gap from the cathode.
α	First Townsend ionization coefficient.
β	Ionization frequency.

β'	Effective ionization frequency (taking into account electron losses).
γ	Secondary emission coefficient in the presence of a magnetic field.
γ_i	Secondary emission coefficient for ion bombardment in the absence of a magnetic field.
Δ	Distance measure of magnetic field line bowing (Fig. 20).
$\overline{\epsilon}$	Mean electron energy.
θ	Angle between the electric field and the perpendicular to the magnetic field.
$\lambda_{c.e.}$	Mean free path for resonant charge exchange of H_2^+.
ν_c	Electron-neutral collision frequency for momentum transfer.
$\sigma_i(v)$	Cross section for ionization by electron impact.
τ	ν_c^{-1}.
ω_b	Electron cyclotron frequency.

REFERENCES

1. L. B. Loeb, Handbuch der Physik (Springer-Verlag, Berlin, 1956), Vol. XXII, p. 445.
2. F. Llewellyn Jones, Handbuch der Physik (Springer-Verlag, Berlin, 1956), Vol. XXII, p. 1.
3. J. M. Meek and J. D. Craggs, Electrical Breakdown of Gases (Oxford University Press, 1953).
4. R. C. Fletcher, Phys. Rev. 76, 1501 (1949).
5. M. J. Bernstein, Phys. Rev. 127, 335 (1962).
6. M. J. Bernstein, Phys. Rev. 127, 342 (1962).
7. G. A. Pearson and W. B. Kunkel, Phys. Rev. 130, 864 (1963).
8. W. P. Allis, Handbuch der Physik (Springer-Verlag, Berlin, 1956), Vol. XXI, p. 404.
9. G. A. Pearson and W. B. Kunkel, Electron-Energy Distributions and Ionization Rates in Hydrogen with Crossed Electric and Strong Magnetic Fields, Lawrence Radiation Laboratory Report UCRL-10366, Sept. 1962.
10. L. B. Loeb, Basic Processes of Gaseous Electronics (University of California Press, Berkeley, 1955).
11. H. A. Blevin and S. C. Haydon, Austr. J. Phys. 11, 18 (1958).
12. D. J. Rose, Phys. Rev. 104, 273 (1956).
13. D. E. Golden, H. Nakano, and L. H. Fisher, Phys. Rev. 138, A1613 (1965).
14. W. Bleakney, Phys. Rev. 35, 1180 (1930).
15. H. B. Gilbody and J. B. Hasted, Proc. Roy. Soc. (London) A238, 334 (1957); W. H. Cramer, J. Chem. Phys. 35, 836 (1961).
16. D. J. Rose, J. Appl. Phys. 31, 643 (1960).
17. J. Fletcher and S. C. Haydon, Austr. J. Phys. 19, 615 (1966).
18. A. von Engel and M. Steenbeck, Elektrische Gasentladungen (Springer, Berlin, 1932), Vol. 1, p. 116.
19. P. F. Little, Handbuch der Physik (Springer-Verlag, Berlin, 1956), Vol. XXI, p. 574.
20. A. G. Englehardt and A. V. Phelps, Phys. Rev. 131, 2115 (1963).